



UNIVERSITAT
POLITÈCNICA
DE VALÈNCIA



SAPIENZA
UNIVERSITÀ DI ROMA

SAPIENZA - UNIVERSITÀ DI ROMA

FACOLTÀ DI INGEGNERIA CIVILE E INDUSTRIALE

FINAL DEGREE THESIS:

**EXPERIMENTAL STUDY OF THE
COANDA EFFECT IN A WATER JET
USING PARTICLE IMAGE
VELOCIMETRY**

A Thesis submitted by Héctor Llorca Llorca

2018

Supervised by:
Giovanni Paolo Romano

Page intentionally left blank

*Dedicado a
mi familia
por todo el apoyo que me han dado hasta llegar aquí*

Acknowledgement

I would like to thank my family, in special to my brother, Salvador Llorca, for its follow-up during the development of the thesis and all his support advice and help during my whole life.

I am also grateful to my tutor for this project, Giovanni Paolo Romano. I would like to thank him for his advice, the time he has devoted to controlling the development of the experiment, for proposing solutions to the adversities that have arisen and in general for his always kind support.

Then I would also like to mention the people that have worked in the *Laboratorio di Fluidodinamica* at Sapienza University during my stay there. A special mention to Dario Spano, the master degree student who I worked with for the whole experiment.

Finally, I would like to thank my friends, those from my city, those from the university in Valencia and those I have done during the Erasmus experience, for making it easier for me to get here. Special thanks to Alberto Herrero and Iván Valencia for showing constant interest in my progress and their spirits and advice during hard times.

Abstract

Coanda effect is a really relevant fluid phenomenon that is difficult to study analytically due to several interacting effects. The experimental study is, therefore, an adequate solution to face it. Motivated by its numerous applications, a parametric study of the Coanda effect in a water jet is carried out. The changing parameter is the position of a wall that forces the jet to deviate. In particular, the study is effectuated for three, four and five jet width distances from the outlet.

As we will need some calibration before the study and also for comparisons, the study of the Free jet, at same Reynolds and Froude numbers, has been carried out. The results of this study indicate that the setup is well calibrated and it is possible to measure correctly the Coanda jet.

The Coanda jet experiment shows that the presence of the wall generates a big influence in the jet and forces it to move towards the wall. It is examined that, the farther the wall is, the farther the reattachment point appears. In particular, it follows a slightly non linearly relationship.

All this study has been done by the Particle Image Velocimetry technique, which has proven to be adequate to obtain all the desired information.

Contents

Acknowledgement	ii
Abstract	iii
List of Figures	vi
List of Tables	ix
Nomenclature	x
1 Introduction	1
1.1 Coanda effect	1
1.1.1 Configuration analogy	4
1.2 Applications of Coanda effect	5
1.2.1 NOTAR helicopters	5
1.2.2 Coastal engineering	7
1.3 Adimensional numbers	7
1.4 Free jet	8
1.5 Targets	10
2 Experimental setup	12
2.1 Basic setup	12
2.2 Assembly phases	14
2.3 Component specifications	18

2.3.1	Tracer particles	18
2.3.2	Camera	20
2.3.3	Flowmeter	22
2.4	Experiment Configurations	23
3	Analysis method	25
3.1	Theoretical background	25
3.1.1	Particle Image Velocimetry (PIV)	26
3.1.2	Particle Tracking Velocimetry (PTV)	26
3.2	PIVlab software	27
4	Free jet experience	31
4.1	Configuration	31
4.2	Results	32
5	Coanda Jet experience	46
5.1	Configuration	46
5.2	Results	47
5.2.1	Reattachment length	67
6	Conclusions	73
6.1	Further work	74

List of Figures

1.1	Visualization of Coanda effect (Wikipedia Coanda effect)	2
1.2	Wall jet schematic drawing	3
1.3	Flow characteristics behind a BFS (Rajasekaran, 2011)	4
1.4	Coanda effect applications examples	5
1.5	Operating principle of NOTAR (Wikipedia NOTAR)	6
1.6	Free jet diagram (Aloysius and Wrobel, 2009)	9
1.7	Free jet longitudinal velocity profile (Tian et al., 2012)	10
2.1	End of the table (V shape) schematical drawing	13
2.2	Table assembly result	15
2.3	Pump with bypass valve configuration	16
2.4	Hydraulic scheme	17
2.5	Structure configuration	18
2.6	Checkerboard positions for the analysis	21
2.7	Image error bar plot	22
3.1	Example of taken images	28
3.2	Example of Pivlab results	30
4.1	Table configuration for free jet	32
4.2	Free jet vector field	32
4.3	Free jet velocity u component	33
4.4	Free jet velocity v component	34

4.5	Free jet vorticity field	34
4.6	Free jet reynolds stress distribution	35
4.7	Free jet u component standard deviation	36
4.8	Free jet v component standard deviation	36
4.9	Free jet u component skewness	37
4.10	Free jet v component skewness	38
4.11	Free jet u component flatness factor	39
4.12	Free jet v component flatness factor	39
4.13	Free jet velocity u component profiles	40
4.14	Free jet velocity u component profile at the outlet	41
4.15	Free jet vorticity profiles	42
4.16	Free jet Reynolds tensor profiles	43
4.17	Free jet dimensionless velocity profile (Abramovich et al., 1984)	43
4.18	Free jet reynolds stress profile (Kuang et al., 2001)	44
4.19	Free jet velocity PIV results (Mi et al., 2007)	44
4.20	Free jet vorticity PIV results (Miozzi et al., 2010)	45
5.1	Table configuration for Coanda jet	47
5.2	Coanda jet vector field	48
5.3	Coanda jet velocity u component	50
5.4	Coanda jet velocity v component	51
5.5	Coanda jet vorticity field	53
5.6	Coanda jet Reynolds tensor distribution	54
5.7	Coanda jet u component standard deviation	55
5.8	Coanda jet v component standard deviation	56
5.9	Coanda jet u component skewness	58
5.10	Coanda jet v component skewness	59
5.11	Coanda jet u component flatness factor	60
5.12	Coanda jet v component flatness factor	61
5.13	Coanda jet velocity u component profiles for $\tilde{H} = 3$	62

5.14	Coanda jet velocity u component profiles for $\tilde{H} = 4$	63
5.15	Coanda jet velocity u component profiles for $\tilde{H} = 5$	63
5.16	Coanda jet vorticity profiles for $\tilde{H} = 3$	64
5.17	Coanda jet vorticity profiles for $\tilde{H} = 4$	65
5.18	Coanda jet velocity vorticity profiles for $\tilde{H} = 5$	65
5.19	Coanda jet Reynolds tensor profiles for $\tilde{H} = 3$	66
5.20	Coanda jet Reynolds tensor profiles for $\tilde{H} = 4$	66
5.21	Coanda jet velocity Reynolds tensor profiles for $\tilde{H} = 5$	67
5.22	velocity u component along the wall for $\tilde{H} = 3$	68
5.23	velocity u component along the wall for $\tilde{H} = 3$ (zoomed)	69
5.24	velocity u component along the wall for $\tilde{H} = 4$	70
5.25	velocity u component along the wall for $\tilde{H} = 4$ (zoomed)	70
5.26	velocity u component along the wall for $\tilde{H} = 5$	71
5.27	velocity u component along the wall for $\tilde{H} = 5$ (zoomed)	71
5.28	Comparison of the experimental results with expression (1.1)	72

List of Tables

2.1	Tracer particles mechanical properties	19
2.2	Camera characteristics used	20
2.3	Measurement matrix of combinations	23
5.1	Reattachment position for the different configurations	68

Nomenclature

Acronymus

CFD	Computational fluid dynamics
CE	Coanda effect
NOTAR	No tail rotor
BFS	Backward Facing Step
PDF	Probability Density Function

Variables

\bar{U}_0	Average output speed (m/s)
h_w	Wall distance respect to the jet centre (m)
x_R	Reattachment point (m)
β	Wall inclination angle respect to the jet centre (deg)
W	Width of the inlet channel (m)
\tilde{x}	Adimensional length in x direction
\tilde{y}	Adimensional length in y direction
\tilde{H}	Adimensional wall length
Re	Reynolds number
Fr	Froude number
ν	kinematic viscosity (m ² /s)
g	Acceleration due to gravity (m/s ²)
\bar{U}_x	Local maximum velocity (m/s)
τ_s	Particle relaxation time (s)
d_p	Particle diameter (m)
ρ_p	Particle density (kg/m ³)
μ	Dynamic viscosity (Ns/m ²)
h	Water profundity (m)
Q	Flow rate (l/min)
N_p	Number of particles

r	Characteristical dimension for PIV (μm)
r_m	Mean distance between particles (μm)
N	Number of vector fields
σ	Standard deviation
s	Skewness
K	Flatness factor

Chapter 1

Introduction

The complexity of the behaviour of the fluid makes the experimental experience, together with the CFD analysis, a mainstay in order to have a good understanding of the various fluid dynamics phenomena.

Over time, the development of experimental techniques made possible to obtain better results with more precision and reliability. Thanks to this, a great improvement in fluid dynamics applications has been carried out.

One of the important phenomena in turbulent flows is the Coanda effect that has been applied in several fields during the last years. It is a really relevant effect that has allowed an important development in engineering besides being very instructive.

The objective of this work will be to determine the influence of the presence of a wall in the deviation of a water jet that is, the principles of the Coanda effect

1.1 Coanda effect

The known as Coanda effect is a fluid phenomenon that was discovered by the Romanian inventor Henry Marie Coandă. The observation was that a fluid tends to deflect towards a wall and adhere to it due to the presence of the same wall (Von Glahn, 1958).

This effect can be explained because of when a jet is near a surface, pressure forces are generated, which change the path of the fluid due to the existing depression between the jet and the surface. Since the solid surface avoids flux in the area between the fluid and the wall a decrease of pressure is produced

in that area in respect to the other side of the jet. The flow near the surface is accelerated and the resultant pressure gradient generates a force towards the wall (Ahmed et al., 2017). This happens for any shape of surfaces (rectilinear, tangential, circular)(Ahmed et al., 2017).

This phenomenon is graphically represented in Figure 1.1 and it is valid as much for gases as for liquids.

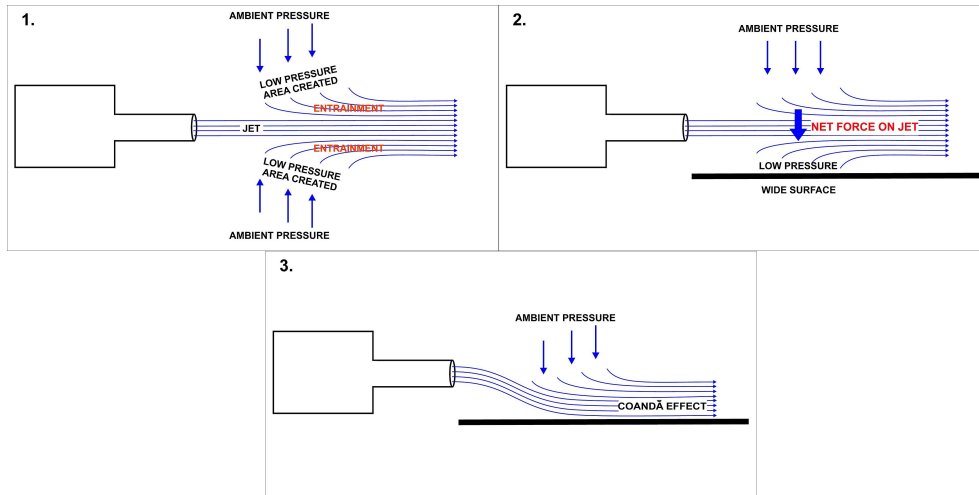


Figure 1.1: Visualization of Coanda effect (Wikipedia Coanda effect)

In this thesis, the effect of an incompressible turbulent jet with free surfaces will be studied. This jet will exit from a bidimensional channel with a nearly constant velocity U_0 in a water table where exists a lateral wall placed in a parallel way at a distance (h_w) of the centre of the jet. This configuration will produce a deflection in the jet and it will be possible to identify the reattachment point (x_R) known as the point where the flow adheres to the wall (see Figure 1.2). After that, downstream of x_R , the jet will have a behaviour of Wall Jet that has been discussed by Glauert (1956) and it can be of a particular interest in many aeronautical applications (Eaton and Johnston, 1981). Instead, upstream of that point a recirculating zone is created.

There are some previous studies and experiments investigating different geometrical configurations and its impact on the reattachment length (Trancossi, 2011). One of the most important parameters that will be studied in this thesis is the h distance. Various experimental studies have determined that the reattachment length is slightly non linearly dependent on the wall distance. An empirical law has been formulated by Nasr and Lai (1998) that

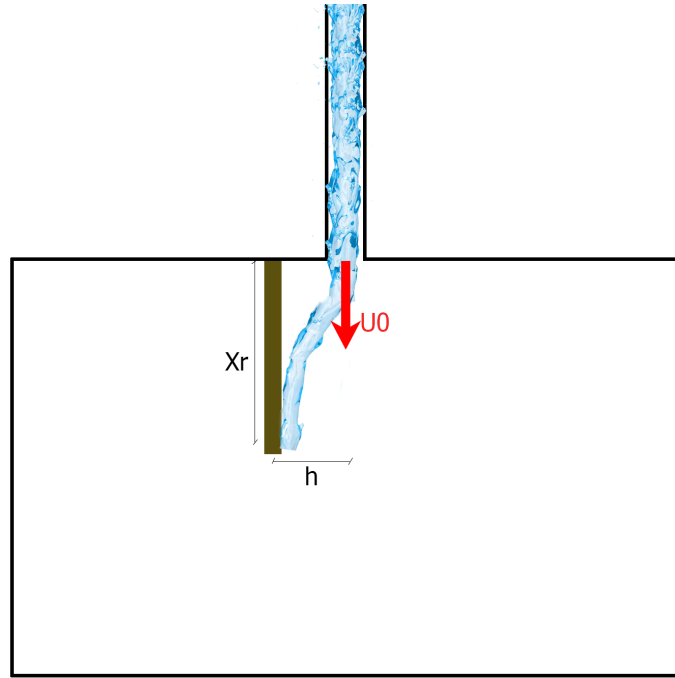


Figure 1.2: Wall jet schematic drawing

shows the following relationship:

$$\tilde{x} = 2.632 \tilde{H}^{0.851} \quad (1.1)$$

Where \tilde{x} is the adimensional length in x direction and \tilde{H} is the adimensional wall distance. Both dimensionless with the output width.

In this study, this will be experienced with good precision in order to confirm the various authors' experiences.

Another interesting studied parameter by the scientific community is the inclination of the wall (β) in relation to the output of the channel. In that case, it is concluded that when higher is the inclination higher is the length of the reattachment (Nasr and Lai, 2010). For timing motives, this won't be experienced in this thesis but it is a good further work that should be taken into account.

Then, there are other two parameters that have to be taken into account ,namely, the adimensional Reynolds and Froude numbers. As in practically any fluid phenomenon, the variation of some adimensional parameters could change the behaviour of the study case. For that reason it is important to

carry out a study of these parameters in order to verify it and how results change.

1.1.1 Configuration analogy

For a better comprehension of any phenomenon, it is important to search if there is any other similar case which enables us to establish an analogy. This will make it possible to establish a first prognosis of what we can expect in our study.

A good analogy that we can find in this effect is the known as backward facing step (BFS). This configuration consists of a conduit that has an expansion due to the presence of a step of a certain height H .

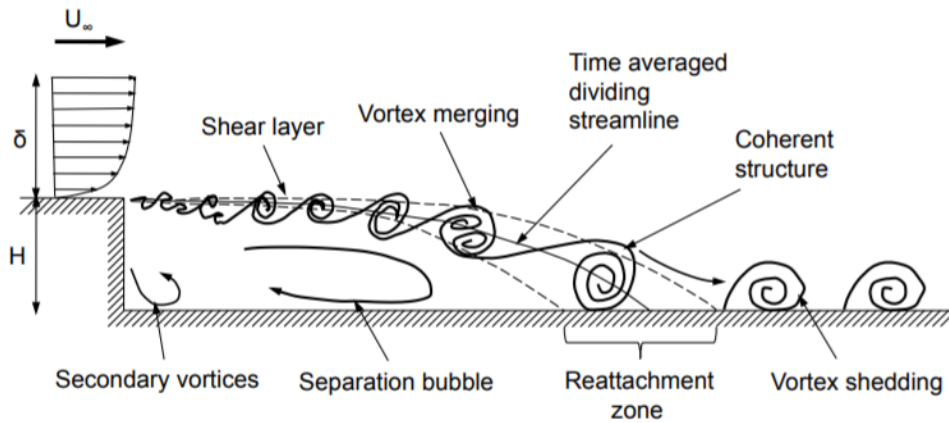


Figure 1.3: Flow characteristics behind a BFS (Rajasekaran, 2011)

As we can see in Figure 1.3 there is a reattachment zone and also a recirculating zone exists before the adherence zone. This will be influenced by the relation between the channel dimension (δ) and the height of the step. Reynolds number will take part also in the development of this flow until values of 3000 (Rajasekaran, 2011). In the case where H is so high respect with δ , the flow will not note the presence of the wall and will evolve in a free mode (Biswas et al., 2004). Having this in mind, a similar effect might happen in the experiments carried out in this thesis if the position of the wall is far from the output channel.

1.2 Applications of Coanda effect

This experience can be used in a large number of applications. The first time it was used was by Coanda, although with a different purpose than expected. He used some plates to deflect the hot air produced by the engine of a airplane, nevertheless the hot flow was conducted directly to the wooden fuselage and the aircraft was destroyed (Englar, 2005).

Nowadays it is possible to see CE in mostly of fluid dynamics devices. The most known are the applications of car engines exhaust, NOTAR helicopters, used as a way to increase the lift on a plane, improve propulsion systems and in coastal engineering (Lalli et al., 2010).

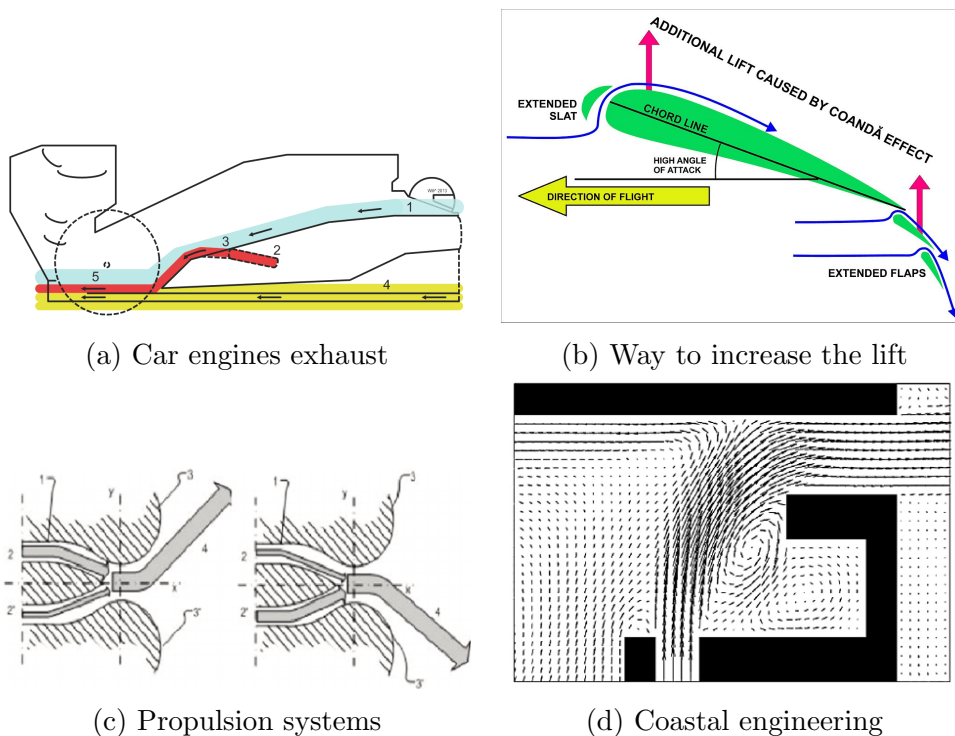


Figure 1.4: Coanda effect applications examples

1.2.1 NOTAR helicopters

An helicopter is a wing rotatory aircraft which can take-off and land in a vertical way. Its lift and thrust are made by a rotor of two or more blades. When the helicopter is in the air it experiences a moment, due to the engine, that tends to rotate the helicopter in its vertical axis in the opposite direction

of the rotor movement. This moment needs to be compensated by another one that stabilizes the aircraft. Traditionally this has been counterbalanced by another small rotor called tiltrotor, that taking advantage of the law of equilibrium of moments generates the necessary torque.

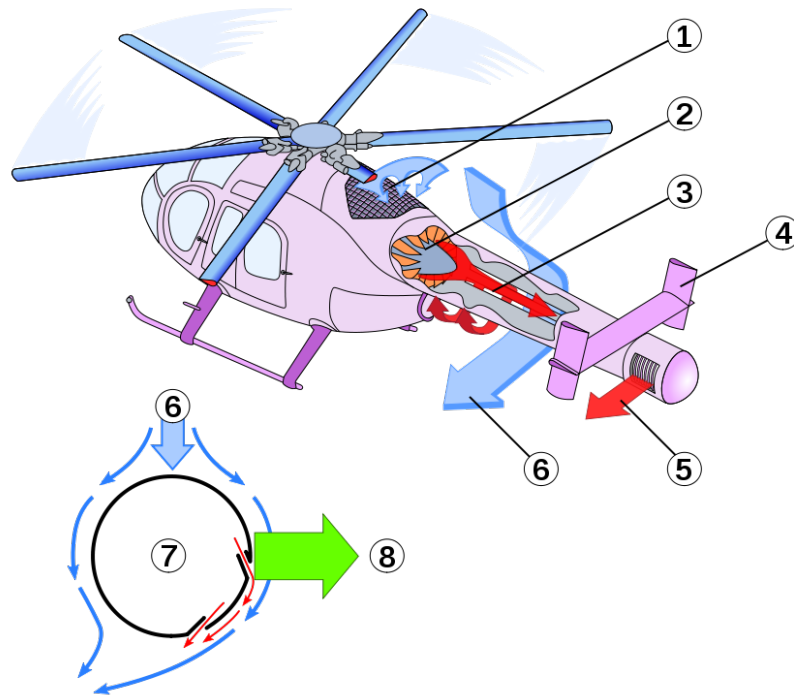


Figure 1.5: Operating principle of NOTAR (Wikipedia NOTAR) (1) Air intake (2) Variable pitch fan (3) Tail boom with Coanda Slots (4) Vertical stabilizers (5) Direct jet thruster (6) Downwash (7) Circulation control tailboom cross-section (8) Anti-torque lift

The NOTAR is a system designed by McDonnell Douglas Helicopter Systems that avoid the tiltrotor. Wringing the CE a low-pressure air zone is generated by a boundary layer flow of air along the tail boom brought about by an internal fan in the tail boom. As we can see in Figure 1.5 the flow deviates in such a way that a force is generated by the pressure difference opposite to the motion of the fuselage.

In particular, a dynamic take, placed under the principal rotor, directs some part of the air coming from the rotor to the inside of the tail. One part of the flow is forced to exit sideways to the tail and follows the profile due to CE,

while the rest is directed to the tailplane. The part of the air that follows the profile generates an asymmetry that produces the balancing force. The other part of the flow is used for a lift enhancement.

1.2.2 Coastal engineering

In the coastal engineering field, CE can be produced between river flows and marine structures. In a simplified point of view, it is possible to consider this interaction as the interaction of a jet with a wall mentioned previously. So these structures are able to modify the flow path in a harbour.

Considering that this change has an impact on the pollution of the shore is important to understand and use CE to improve the environmental conditions.

As an example in Lalli et al. (2010) study, it has studied the distribution of the Pescara and Latina harbours having in mind the possible changes in the important parameters for the CE study. One of the results obtained is that the forcing terms that give rise to CE are the free gradient surfaces related to the vortex generated between the jet and the wall. Also, they observe that if the bottom is so rough or the ratio between horizontal and vertical scale are so large, the CE vanishes.

1.3 Adimensional numbers

It is important to understand the meaning of the adimensional numbers that have any influence in the experiment. A theoretical explanation is given for the better comprehension of the future mention of these parameters.

- Reynolds number (Re): By definition, Reynolds number expresses the relationship between inertia and viscous forces. It is commonly expressed as:

$$Re = \frac{v L}{\nu} \quad (1.2)$$

where v express the fluid velocity with respect to the object and L is a characteristic linear dimension. A high Reynolds number means that the fluid has a large inertia so the viscous effects have a minor repercussion. On the contrary, if the Reynolds number is low the viscous effects have more relevance than the inertia effects. The criterion to

affirm that this parameter is high or low could change in function of the studied application. One of the most common uses of this number is to classify the flows in laminar or turbulent, for example for internal flow it could be considered that a flow with a value less than 2000 is laminar while Reynolds above 5000 could be considered for turbulent flows. However for external applications as for example planes flying at cruise condition the magnitude order of the Reynolds number is often about 10^6 or 10^7 .

- Froude number (Fr): This number expresses the relationship between the inertial forces and gravity forces. Its expression can be changed in function of the application, for shallow water with rectangular cross-sections with uniform depth can be expressed as:

$$Fr = \frac{v}{\sqrt{gd}} \quad (1.3)$$

Where v means the flow velocity and d the uniform depth. One of its uses in free-surface flow is to determine the nature of the flow if a flow is subcritical ($Fr < 1$), critical ($Fr = 1$) or supercritical ($Fr > 1$). Knowing this is possible to make the analogy with the Mach number for airflow regimes.

1.4 Free jet

For this study, it is also important to consider the characteristics of the free jet in order to compare them with the Coanda jet.

To define the measures of the free jet, it is possible to define them in the transversal direction by identifying the points that are equal to 1% of the output velocity. This length increase throughout the longitudinal direction, so the further from the output the checkpoint is, the longer transversal length will the jet have.

Analyzing Figure 1.6, it is possible to identify two different zones, the first one, called flow development region which is the region where the velocity is practically constant and equal to the output velocity (U_0). The second one, where the flow is fully developed, the velocity tends to decrease in the streamwise direction due to the turbulence generated on the boundary of the jet that goes through the interior part of the jet. So in this region, the velocity change from U_0 to 0 when the jet reaches a long length in the x-direction.

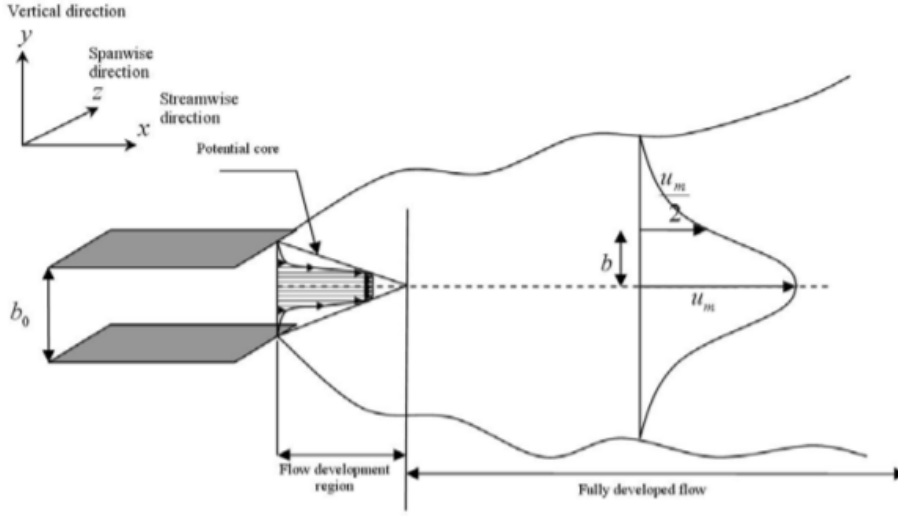


Figure 1.6: Free jet diagram (Aloysius and Wrobel, 2009)

Depending on the characteristics of the jet the development of the velocity decay and the flow spread could change. For turbulent circular jets (Pope, 2000) the following relationship is observed:

$$\frac{\bar{U}_0}{\bar{U}_x} \simeq \tilde{x} \quad \delta(x) = \tilde{y}_{1/2} \simeq \tilde{x} \quad (1.4)$$

Where \bar{U}_x is the local maximum velocity of the jet and $\delta(x)$ is the jet semi-thickness. Looking at the resulted expression it is stated that both the velocity decay and the spread are linear in the x-direction.

For plane jets (Kuang et al., 2001) the following relationships are obtained:

$$\frac{\bar{U}_0}{\bar{U}_x} \simeq \tilde{x}^{1/2} \quad \delta(x) = \tilde{y}_{1/2} \simeq \tilde{x} \quad (1.5)$$

That indicates that in this case the velocity decay is not more linear but increases with the x array.

Another characteristic that should be mentioned is the velocity profile of the jet. Taking a perpendicular line to the jet axis and analyzing the velocity of each point of the line we obtain the velocity profile of the jet. For the longitudinal velocity, as it is possible to see in Figure 1.7, we obtain a parabolic profile centered on the value zero.

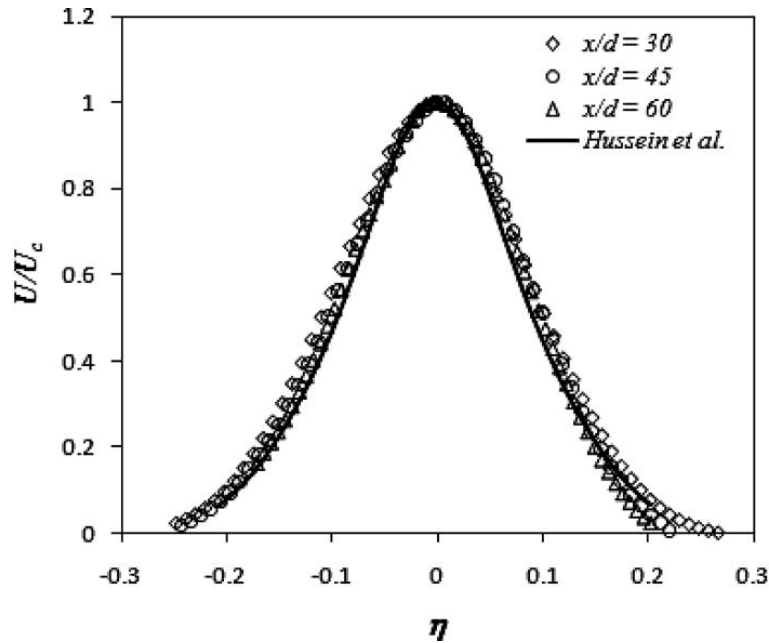


Figure 1.7: Free jet longitudinal velocity profile (Tian et al., 2012)

1.5 Targets

The targets of this thesis can be summarised up as:

- To establish the correct procedure for setting up an experimental water tank with free surface. For the accomplishment of any experimental activity, it is important to prepare in a suitable way the instrumentation of measure. We must be sure that our measures can be taken properly and they are representative. To achieve this target it is necessary to realize a correct setup.
- The study of the free jet flow. Even if this is a well-studied effect, it is interesting to go through it in order to verify that the executed process has been done properly. Also if the used technique has a good precision it is possible to update the bibliography data.
- The study of the Coanda effect, in particular, the influence of the wall distance in the reattachment point. This is the main objective of the experiment.

It is worth mentioning that this thesis is of 12 European Credit Transfer and Accumulation System (ECTS) which is equivalent to a total of 300 hours. Therefore for timing reasons, it is not possible to establish a deep study of the fluid dynamics phenomena prioritizing thus the setup process in order to allow in the future the possibility of accomplishing deep studies without the assembly phase.

Chapter 2

Experimental setup

2.1 Basic setup

In this section it is introduced the basic material used in the experiment, which will be explained in more detail afterwards.

To carry out this experiment, we work with a water tank. This tank is an aluminium base plate of 2 meters per 1.5 meters. The lateral walls are made out of a transparent material in order to allow the visibility inside the water container. It is also needed a channel to introduce the flux jet inside the measurement area. The channel has a width of 5 cm and we will use this length as a reference expressed with the letter W . For making the flow turbulent it is placed a set of spikes in the middle of the channel in a random way. Moreover, two boxes of the same material are located to the exit of the channel moving the outlet point to the centre of the table and assuring that the flow is completely straight at the outlet.

The water used for the experiment is inside an external deposit where an adjustable pump takes it and put it into the tank. The pump is installed with a feedback conduct that redirects part of the water to the deposit in order to regulate better the water flow. Additionally, a flowmeter is installed to give us information about the flow in litres per minute.

Before entering the channel, the water falls down in a small intermediete tank, namely calm camera, allowing us to attenuate the instabilities produced by the pump and passing through a honeycomb in order to achieve a smooth laminar-turbulent transition.

To close the water circuit a gutter is installed in order to make the water

return to the external deposit.

It is also important to regulate the height of the water inside the tank, for that reason, the end of the table has a fixed V shape element so by adding another V shape plate (in this case movable) as shown in Figure 2.1, it is possible to get the required water level. The idea is that, to reach the maximum level (4.5 cm) the movable plate should be located so that its peak coincides with the valley of the fixed plate. On the other hand, for reducing the height, the movable plate should be moved laterally in order to increase the opening, reducing in this way the level of water.

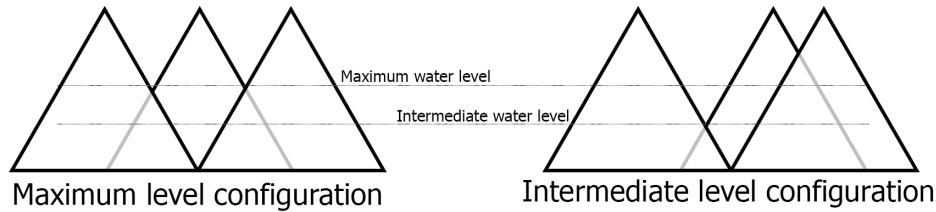


Figure 2.1: End of the table (V shape) schematical drawing

To register the images that will be processed afterwards, we will use a video camera located at the top of the table in a vertical position which will capture the measurement area of approximately 50 x 70 cm.

It is needed to have something that can be registered by the camera and then be analyzed. For that purpose a set of tracer particles of a mean diameter of 250 μm and a density of 0.7 kg/m^3 has been acquired. The selection of this particles is really important for the validity of the experiment and in some later section is justified such selection for this experiment.

Finally, to control the illumination, we used some lamps of 400 Watts of power that illuminate the measurement area. Also, we cover the interesting surface with a fabric avoiding the natural illumination and the reflexion of the general lights that is not possible to control.

2.2 Assembly phases

First of all, as this is an experimental work that took place in a laboratory, is needed to make a general safety course in order to minimize the risk during the assembly and measurement phases. In this case, the Sapienza University has provided a 4 hours course through an e-learning platform.

Then, it is possible to start with the preparation of the setup. The first part is to prepare the naval tank. The most important thing is to achieve the maximum possible levelled surface. As we are studying the deviation of a jet, it is crucial that the initial jet, which is used to compare, is as much straight as possible. Having in mind that the floor is not levelled, we have used some thin steal plates under the legs of the table where the naval tank is supported in order to get it leveled. To measure the level is used Spirit level in every direction until being sure that the objective level is achieved.

Afterwards, as we are working with water, it is important to be sure that there is no possibility of having water losses that can interfere with the measurements and also be dangerous if there is some electrical component near the tank. For that reason, every place where it is possible to have some leak is waterproofed using silicone.

Next, with regards to the tank background, it has to be considered that it is necessary to have it in a black colour so as to avoid the light reflexion. To accomplish this target, it is covered all the surface with a waterproof black cloth. It is sold in pieces of 90 cm wide so it is necessary to put more than one and in some places, there will be an inevitable little joint line.

Finally, it is installed a gutter with an inclination towards an external deposit in order to conduct the water surplus to its origin. In the exit of the gutter, it is possible to put if it is necessary a wire mesh to collect the tracer particles used in the experiment.

In Figure 2.2 we can see an image of the result of this assembly part of the table, wich, if not the most, one of the most important parts.

The next step is to connect the external deposit with the water table. For that, we have to disposition a hydraulic pump. This pump has no power regulation so, for controlling the flow it is used a bypass valve (see Figure 2.3). This way, the pump will take water from the deposit and part of that water will go through the experiment zone and some will be recirculated back to the deposit. This lets us have more precision to work with a precise flow rate than using a simple valve.

Before entering to the water table the water flow passes through a flowmeter

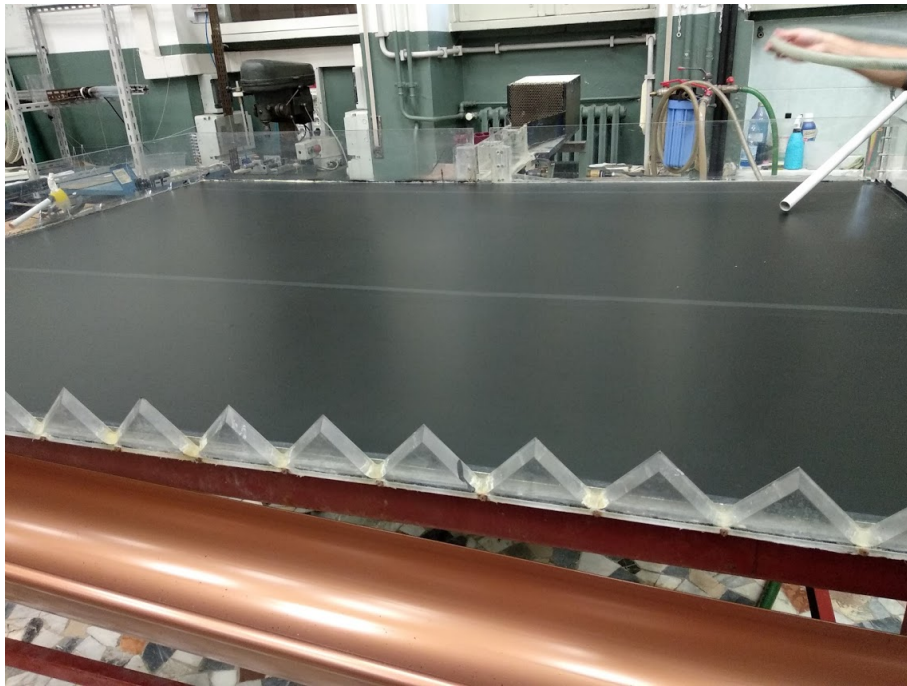


Figure 2.2: Table assembly result

that let us know the flow rate in litres per minute units. This is a very sensitive instrument that must be in a stable zone in order to ensure that the lecture has as minimum disturbances as possible. Then, from the flowmeter exit, a final tube is connected to the input of the calm camera. In this case, the hydraulic circuit is closed. In Figure 2.4 we can see a hydraulic scheme of the configuration achieved at this point.

Now there is a closed water circuit with the capacity to regulate the jet output velocity through the flow rate. At this point, it is necessary to create the set up for the images registration of the fluid phenomena.

The first step is to build a robust structure that reaches the camera in a vertical point of view and let us install a light distribution for controlling the illumination conditions of the experiment. The structure must be rigid because any small oscillation can create a disturbance in the images taken by the camera.

We must bare in mind that the camera position will be changed in the middle of the experiment. For the free jet experiment, we need the centre of the camera aligned to the output centre of the flow, as the jet evolves symmetrically. For the Coanda jet instead, we need the camera displaced to the wall



Figure 2.3: Pump with bypass valve configuration

position, as the jet will deviate more than the 50 cm of the measuring area that we will have. To solve that, the structure that holds the camera has a fixed base, which at the same time, a second part of the structure, where the camera is attached from, can be moved along the transversal direction of the jet.

The illumination is configured with four lamps of 400 W power for each lamp (total power of 1200W) distributed for the better illumination of the measuring area. It is important to not overexpose the image so as the lamps are quite powerful it is necessary to have them at a certain distance. The configuration must be also made in a way that avoids as much as possible the effect of shadows. For that reason, it is important to have light in both directions (transversal and longitudinal). After doing different tests, it is decided to put two of them at lateral sides (one for each side) for having transversal illumination, and the other two at the same side, downstream, with a certain angle to produce a component of transversal and longitudinal illumination.

In Figure 2.5 we can see the final structure configuration. As we can see the structure has a cube shape reinforced with links between the different parts. The vertical structure at the top is the place where the camera is fixed. It is possible to see also how the camera can be displaced along the horizontal crossbar.

It is important to make sure that any part of the structure can be seen in the

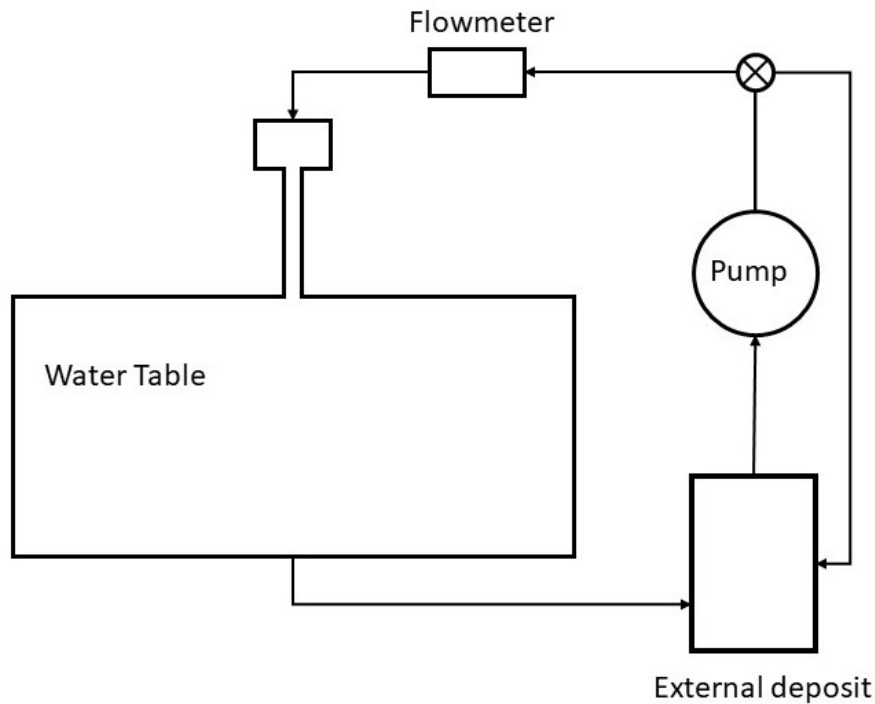


Figure 2.4: Hydraulic scheme

images taken by the camera. For that reason, the camera is not attached directly to the vertical bar. Also as the measurement area is so big, it is necessary to put the camera in an elevated point, thus, a vertical bar is needed to achieve the correct height.

In addition to this, to ensure that the flow will be completely developed as turbulent, not in the transition phase, some spikes are set in the middle of the channel and also the output is elongated by two boxes of the same material that displaces the output 30 cm downstream.

Finally, the whole table is covered by a black fabric that avoids the light passing through it. This is done to ensure that the light conditions are always the same and no reflexion due to the natural or laboratory light can be seen. At the same time, the cable connexion between the camera and the computer is put in order to control the camera with its software.



Figure 2.5: Structure configuration

2.3 Component specifications

At this point we proceed to explain in more detail the specifications of the most important components used for the experiment, namely the tracer particles, the camera and the flowmeter.

2.3.1 Tracer particles

The measurement of any magnitude in this experiment is based on two fundamental dimensions that are length and time. In a flow, it is not possible to determine these dimensions so it is necessary to use something that allows us to identify them. The solution is to use tracer particles which are easily identifiable. So the measurement consists of the study of the length and time of these particles. For the correct experimentation, a set of fluid mechanical properties have to be accomplished.

One of the most important sources of error is the effect of gravitational

forces due to the density difference between fluid and particle. It is possible to identify a relaxation time that has the following expression (Raffel et al., 2007):

$$\tau_s = d_p^2 \frac{\rho_p}{18\mu} \quad (2.1)$$

This magnitude can be used as a measure for the tendency of particles to attain velocity equilibrium. This value must be less than the large structure turnover time in order to ensure that large structures are well resolved. The large structure turnover time can be defined as:

$$t_L = \frac{W}{U_0} \approx 0.5 \text{ s} \quad (2.2)$$

Where W has a value of 0.05 m, defined previously, and U_0 we use 0.1 m/s as a first approximation.

In Table 2.1 it is possible to see the characteristics of the particles used in this experiment. We select the particles OMEGA-SPHERES®W of the Osthoff Omega Group.

Material	Ceramic
Mean diameter	250 (μm)
Density	700 (kg/m^3)

Table 2.1: Tracer particles mechanical properties

As the dynamic viscosity of the water is around the magnitude order of $\mu = 10^{-4}$ the particle relaxing time has a value of approximately:

$$\tau_s \approx 2.5 \cdot 10^{-3} \text{ s} \quad (2.3)$$

This value is much less than t_L so it is possible to affirm that large structures are well resolved.

Another important characteristic is that the particles must have good light reflectance. The camera can see the light reflexion in the particles so it is really important that the particles produce a good one. About the shape, it has to be a spherical shape in order to achieve a regular reflection. For that reason, the particles used are nearly white spherical particles.

2.3.2 Camera

The camera is another fundamental part of the experiment. The quality of the images taken by the camera will determine also the analysis quality. The model used in this experiment is the AVT PIKE F-421B with an objective Canon 25mm. The software used for controlling the camera is SmartView of Allied Vision Technologies company. The technical characteristics of the camera used in this case are reported in Table 2.2.

Picture size	1600 (H) x 1200 (V)
Resolution depth	8 bit
Frame rate	15 fps
Shutter speed	10 μ s
Spatial resolution	0.438 mm
Time resolution	67 ms

Table 2.2: Camera characteristics used

The images will be taken in dark conditions so it is important to have a camera that can have a good behaviour in these conditions and this Pike model with the objective used can do it.

As a length of 70 cm is cover by 1600 pixels we can determine the particle size in pixels. The calculus is the following:

$$l_p = \left(\frac{7 \cdot 10^{-1}}{1600} \right)^{-1} 2.5 \cdot 10^{-4} = 0.57 \text{ px} \quad (2.4)$$

We can note that the particle size is less than one pixel. This could be a problem for the identification of the particles as maybe the software can't recognize the particle but we must have in mind that the particles will tend to aggregate between them so the camera will see particles of more than 1 pixel.

The images are taken in a TIFF format with a low compression. The ideal case is to take photos with no compression but the software used doesn't give the possibility to record images with no compression, so the option used is the best of our range of possibilities.

Then, it is important to pay attention to the software configuration. This software is not created to register a long set of images. That means that if a fast mode configuration for a big amount of images is set, it is probable that

there will be some pictures that will not be recorded. To avoid this problem, it is fundamental to select a high value of buffer. Increasing the buffer value means that some images are recorded in the RAM memory for the posterior recording in the hard disk.

Then, it is decided to take 1000 images for the analysis so it is important to set a multishot in the software for being sure that we obtain the correct images number.

Camera calibration

It is important to be sure that the camera has no relevant error for the experiment. To ensure that we can use the camera is crucial to realize a calibration process before using it.

For the calibration, we take images of a planar checkerboard, with a known length of 30 mm for each square side, in different positions and then, using the Matlab App Camera Calibrator, we can study the error. Looking at Figure 2.6 we can see the different checkerboard configurations used. There are 21 images to increase the calibration precision and it has taken lots of different angles and distances.

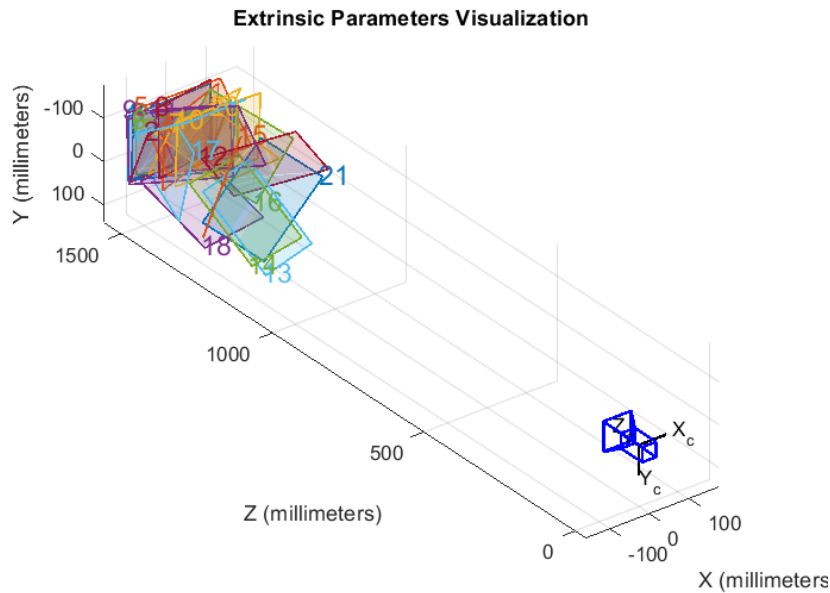


Figure 2.6: Checkerboard positions for the analysis

To calculate the mean reprojection error it is necessary to select the corners of each image. Then, when the calibration starts, the software calculates the corners using a specific algorithm. So the reprojection error is the difference in pixels of both quantities. This generates an error of each image and to obtain the overall mean reprojection error, it is enough making the average of the error of all the images.

The results indicate (see Figure 2.7) that the overall mean error is about 0.23 px, that is acceptable because is less than one pixel and even is less than the half-length of a single particle so it is possible to accept the images taken by this camera.

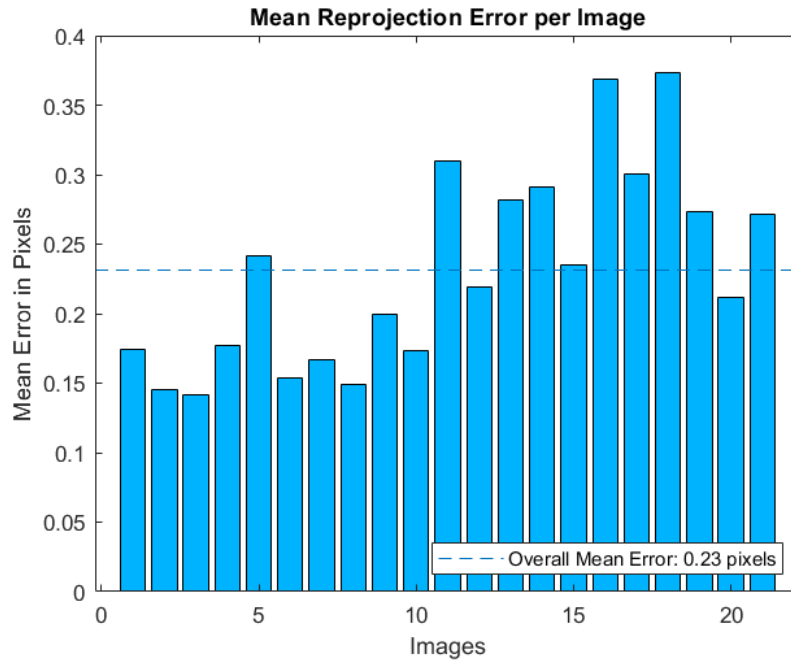


Figure 2.7: Image error bar plot

2.3.3 Flowmeter

As previously mentioned, the Reynolds number could be important in the experiment and for that, it must be a manipulated variable. To control the Reynolds it's necessary to have a regulation in the flow rate. This is possible throughout the variation in the valve opening. But any of these is possible if it is no information of the precise flow rate value and, to obtain it, it is

necessary to have a flowmeter.

The flowmeter used is the Electronic ultrasonic flow-sensor UQS 7 of Barksdale. This sensor has an error of 2.5% and lets us know the flow rate in litres per minute.

Once we know the flow rate value it is possible to obtain the velocity and with it the Reynolds number.

$$U_0 = \frac{Q}{A} \left(\frac{l}{m^2 \text{ min}} \cdot \frac{1m^3}{1000l} \cdot \frac{1\text{min}}{60s} \right) = \frac{Q}{W h} \quad (2.5)$$

So the Reynolds number can be expressed as:

$$Re = \frac{U_0 h}{\nu} = \frac{Q}{W \nu} \quad (2.6)$$

With this expression, we can calculate that for example to obtain a Reynolds value of 5000 it is necessary to have a flow rate of 15 litres per minute. This value is inside the range of our flowmeter that is configurated to read values from 0.4 to 100 l/min.

2.4 Experiment Configurations

This experiment has taken part in two different configurations. One for the Free jet and the other for the Coanda jet. For the free jet, there are two variables that we can change for the study (Reynolds and Froude) while in Coanda jet there are three parameters (Reynolds, Froude and Wall distance).

In Table 2.3 it is collected the combination of measures that are taken for this particular experiment, having in mind that it is possible to realize as many combinations as it is considered necessary in function of the available time and targets.

Re	Fr	\tilde{H}
Free Jet		
5000	0.17	
Coanda Jet		
5000	0.17	3
		4
		5

Table 2.3: Measurement matrix of combinations

We realize in total 4 measures in total. If we make a revision of the available literature (Miozzi et al., 2010) we observe that for our range the Reynolds value has small relevancy in the result so it is considered to not change it for this experiment.

For the free jet is considered to use one value of Froude number, the same value as is used in the Coanda jet. As this is not the study target it is not necessary to realize more measures.

About Coanda jet, it is modified the wall length three times for seeing in a good way its effect.

To achieve the Froude number, at this Reynolds condition, the water depth has to be of 4.5 cm.

Also, the wall will be displaced a minimum of 15 cm from the jet centre up to 25 cm at the maximum case.

Chapter 3

Analysis method

In this chapter, it is explained the analysis technique of the experiment. The good knowledge of the experimental analysis method determines the quality, time and validity of the results obtained from it.

3.1 Theoretical background

The target of the measurements is to obtain the velocity field of the fluid dynamic phenomenon. There are various techniques to obtain it, each one with its own characteristics. We must know which characteristics are interesting for our experiment, in general for this type of experiment we need:

- Global type: We need to measure the entire phenomenon, not a specific part or region of it.
- Non-intrusive technique: It is important to use a technique that cannot modify the final result. If we want to study a specific behaviour with specific conditions we must not have any disturbance that alters the result.
- Linearity: It is important to have linearity between the measured magnitude and the unknowns.
- Good spatial and time resolution: The resolution must be adequate for the physical phenomenon studied.

Taking all of them into account, there are two techniques that fit well with

our requirements namely, Particle Image Velocimetry (PIV) and Particle Tracking Velocimetry (PTV).

3.1.1 Particle Image Velocimetry (PIV)

The PIV technique is a linear non-intrusive optical technique that allows the measurement of at least two components of the velocity field with a good spatial and temporal resolution.

The measuring principle is based on the determination of the tracer particles displacement in a known time interval, noted from the time interval between frames. If there is more than one image of the same particle in a frame it is a case of multi-exposure, instead, if there is a unique image of the same particle in one frame it is a case of single exposure. This depends on the velocity in terms of fps that the acquisition system can achieve.

Another important parameter of the technique is the particle density of the image. We define N_p as the number of particles in one zone with a characteristic dimension r . We also define r_m as the mean distance between particles. To obtain a good PIV analysis we must have as conditions:

$$r_m \ll r \quad ; \quad N_p \gg 1 \quad (3.1)$$

This means that, for a good analysis, we need a high density of particles in the measuring area. For example, a value of $N_p = 10$ is a good order of magnitude in this analysis method (Romano, 2016).

The analysis PIV consists of splitting up the spatial domain in a group of sub-domains wherein each one will be calculated the mean displacement of the particles. For reasons related to the algorithm used, the sub-domains have a square shape with a side length of a multiple of two.

The displacement in each sub-domain is calculated with a bidimensional self-correlation function for multi-exposure or a cross-correlation function for a single exposure.

3.1.2 Particle Tracking Velocimetry (PTV)

The PTV technique is a non-intrusive optical technique. The difference between this method and PIV is that with this technique, we want to obtain the displacement of each particle and not the average between all the particles

in a sub-domain. Therefore, in this method the image it is not divided into sub-domains.

To apply this technique in a good way, it is important to have the following conditions (Romano, 2016):

$$r_m \leq r \quad ; \quad N_p \sim 1 \quad (3.2)$$

As we can see, a low particle density is needed to apply this method. One advantage of this method is that it is possible to have a Lagrangian and Eulerian specification of the flow field while in the PIV, it is only possible to have a Eulerian specification. In any case, the quality of PIV is better than PTV.

As we follow the relative position of the particles in the illuminated area to obtain the information about the velocity field it is necessary to apply an interpolation and other preprocessing techniques while in PIV it is not necessary.

Having this conditions in mind it has been chosen to use the PIV technique for the analysis of the experiment. As we will have low control of particle density and it will be quite high, it is better not to use PTV method.

3.2 PIVlab software

For applying the Particle Image Velocimetry algorithms it is used the Matlab toolbox PIVlab available in Mathworks file exchange page. The tool, created by William Thielicke, is a time-resolved software that is updated regularly with software fixes and new features, therefore, it is considered a good option for this study. One of its advantages is that has a user-friendly graphical user interface that makes easy its use.

An example of the images acquired is represented in Figure 3.1

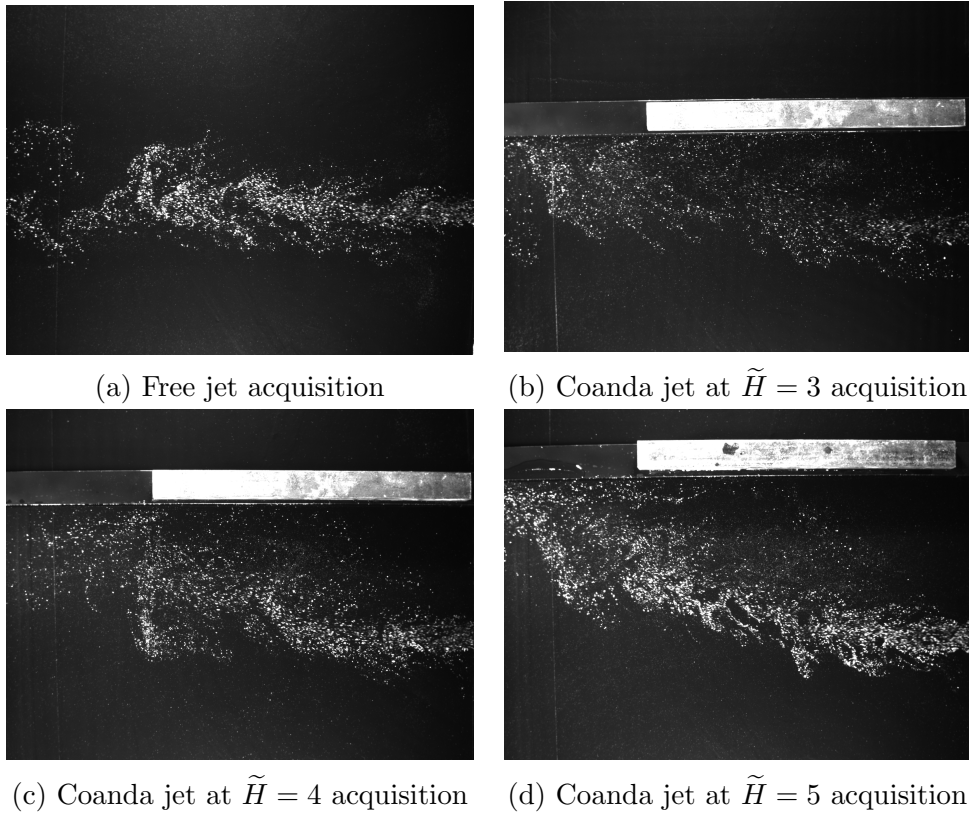


Figure 3.1: Example of taken images

Once obtained the images it is the moment to start a new session in PIVlab to load all the images and realize the analysis. The software only takes an even number of images. In our analysis are taken a total of 1000 images so the software will return 500 vector fields (this number is denoted by N). The more images are analyzed the more rigorous the result will be but at the same time, more time will be needed to finish the analysis. For this reason, it is important to find an equilibrium and after carrying out some tests it was decided to use 1000 images.

Before starting the analysis, it is possible to exclude some areas of the image that do not need to be studied. This is possible with the analysis settings of Exclusions (ROI, Mask) which is an interesting option for the wall studies because we are not interested in what happens behind the wall. In our particular case, it is applied a mask in the images of the Coanda Jet that arrive until the beginning of the wall in order to speed up the analysis time.

About the settings, there are two different correlation algorithms, DCC (single pass direct cross correlation) and FFT window deformation (direct Fourier

transform correlation with multiple passes and deforming windows). In general, the second one produces more accurate results and therefore, it is the selected for our analysis.

Using FFT algorithm the data will be analysed in several passes: The first pass use relative large interrogative windows to make a general reliable displacement analysis. The larger is the area, the better signal-to-noise ratio, but in contrary we obtain less vector resolution. That is why it is necessary to make more passes at smaller areas. This procedure yields a high vector resolution, a high signal-to-noise ratio, and a high dynamic velocity range (Thielicke, 2014). In our case, it is used for 3 passes. For the first one is a pass from a 128 px area to a 64 px area. Then the passes go from 64 to 32 and from 32 to 16 in order to always reduce the area to a half.

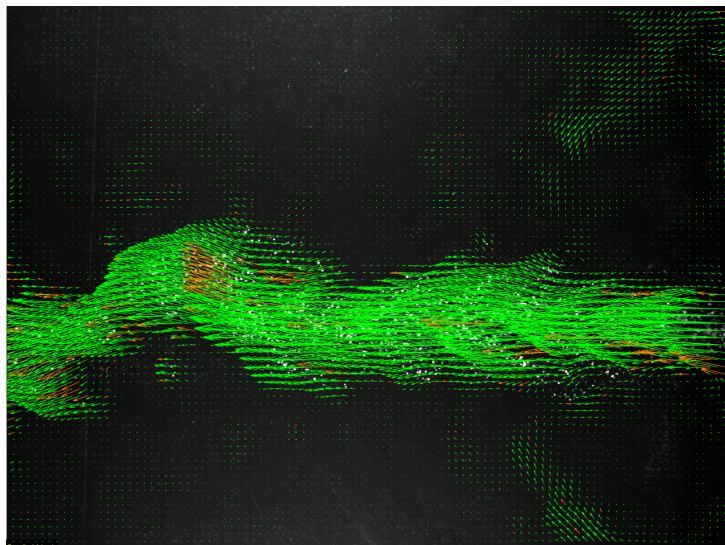
Once the settings are done it is the moment to start the analysis. The analysis will be done automatically and then the vector maps will be created. After the analysis, it is possible to calibrate the values, that is, to set how many meters correspond a pixel. To make the calibration it is enough to take an image, select two known points from it and set its real distance in millimetres, for example, for our images a good choice is the outlet length ($W = 50$ mm) and the time between two images that is the inverse of the fps value, in our case 67 ms.

After the calibration, it is possible to apply a post-processing action in order to clear some erroneous vectors. For that, it is possible to select velocity limits. For example, if all the result appears in a velocity range and a very few vectors have a velocity so distant then it means that are spurious vectors and can be eliminated. Besides, it is possible to apply some filters that reduce the noise data generated in the analysis.

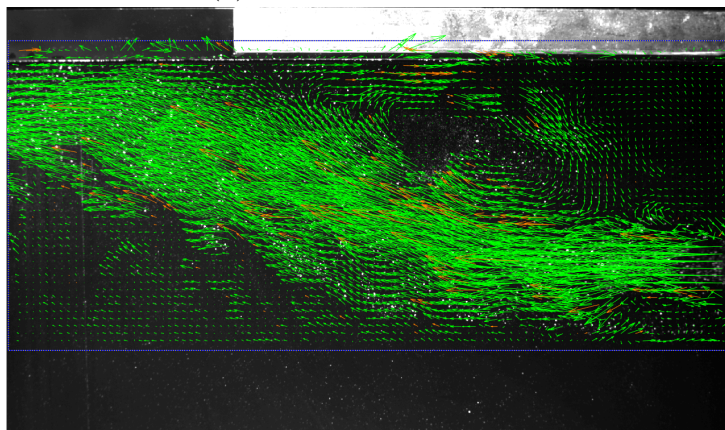
The filters applied in all the analysis that took part in the experiment are the Stedv filter with a Threshold value of 4 and a local median filter with a Threshold value of 4 and an epsilon value of 0.1.

With all of this, it is possible to put all the results obtained with the tool in the Matlab workspace for its processing. Also, the tool can generate some information (an example shown in Figure 3.2) as the vorticity and plot it but, as we want to study more information that the tool generates it is selected to do all the data processing with Matlab.

This procedure is done for all the measures and the results obtained will be shown in the following chapters.



(a) Pivlab free jet results



(b) Pivlab Coanda jet results

Figure 3.2: Example of Pivlab results

Chapter 4

Free jet experience

In this chapter, the results obtained from the free jet experience of the experiment will be analysed. This is used as a preliminary setup and to ensure that all the components work in a correct way.

4.1 Configuration

The Configuration of this experience is easier than the Coanda jet as there are only two variables to set up (flow rate and water height). As previously mentioned, we measure only one condition of Froude and Reynolds. To achieve the value of Reynolds 5000 it is necessary to calculate the flow rate using (2.6):

$$Q = Re W \nu = 15 \text{ [l/min]} \quad (4.1)$$

To obtain the desired Froude value of 0.17 we need the water level height value and the mean output velocity value so we need to solve a system of equations using (1.3) and (2.5). So the necessary values are:

$$h = 0.045 \text{ m} \quad ; \quad U_0 = 0.11 \text{ m/s} \quad (4.2)$$

So, in this case, it is only necessary to set the correct valve opening and the water level. The jet will exit between the two boxes in a straight way as we can see in Figure 4.1.

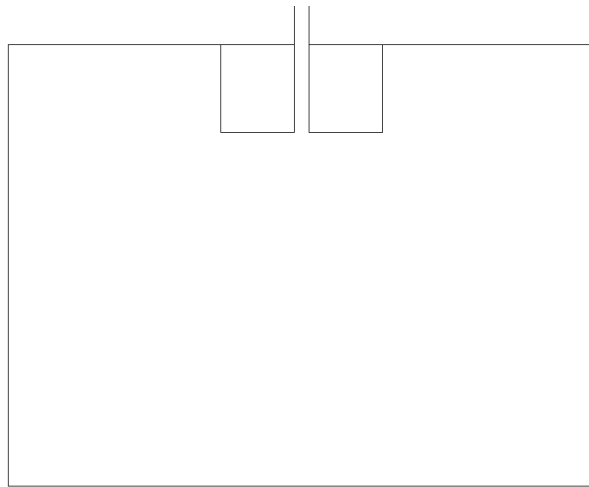


Figure 4.1: Table configuration for free jet

4.2 Results

After doing the analysis a vector field is obtained. This represents the velocity field of the jet. In Figure 4.2 we can see a graphical representation of the resulting vector field.

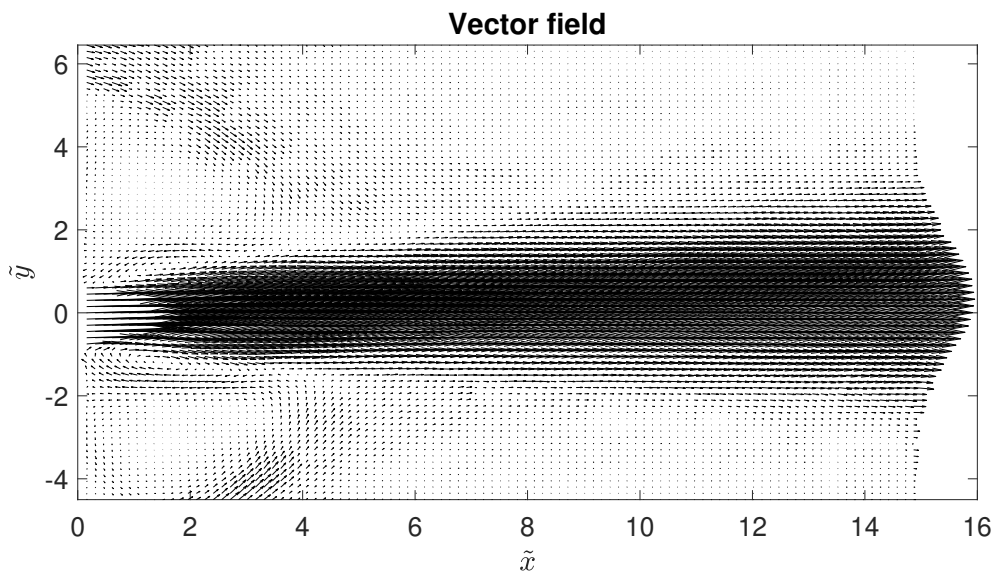


Figure 4.2: Free jet vector field

For the free jet, we can expect a completely horizontal component (u) of the velocity without any relevant vertical component (v). In the vector field, we can observe that in general the vectors do not deviate being enough horizontal. We have to take into account that these are experimental data with small errors. The errors can be produced because the table could have some imperfection that slightly deviates the jet. Also, we are taking the measures in a finite tank whereas the theoretical free jet occurs in an unconfined surface.

These errors can explain the little recirculating that can be observed at the jet output. The Boundary conditions can't be the ideal with the available material. Nevertheless, from a general point of view, we can affirm that the results show the free jet behaviour that we could expect.

With the data obtained it is possible to represent the velocity components (Figure 4.3 and Figure 4.4).

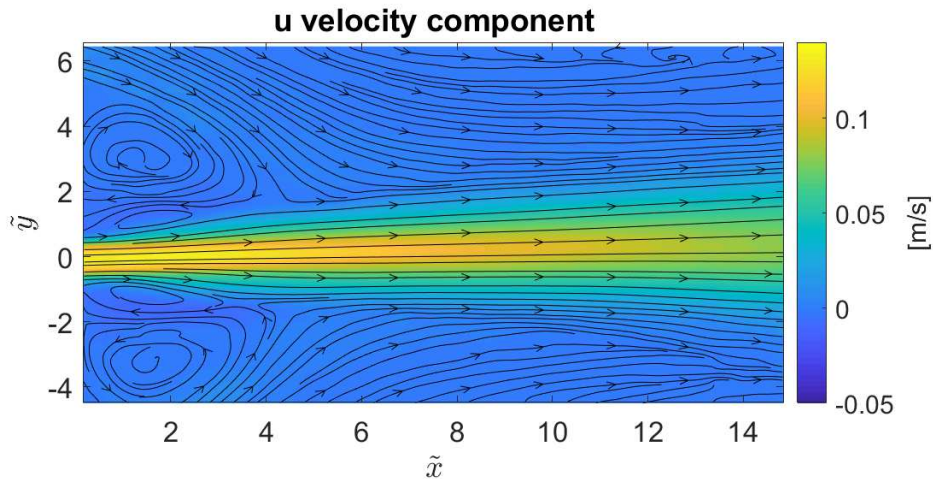


Figure 4.3: Free jet velocity u component

In u velocity plot is overlaped the streamlines in order to clarify the motion of the fluid. In this way, it is easy to identify the recirculating near the output. However, it is possible to appreciate that the jet has a good symmetry that indicates a straight motion. If we see the output velocity value we see that we have a value greater than 0.1 m/s so near of the expected value of 0.11 m/s that produces the desired Reynolds value.

About the vertical component, we can see that practically is near to 0 in the whole area. The value different from 0 is due to the small errors and boundary conditions previously commented.

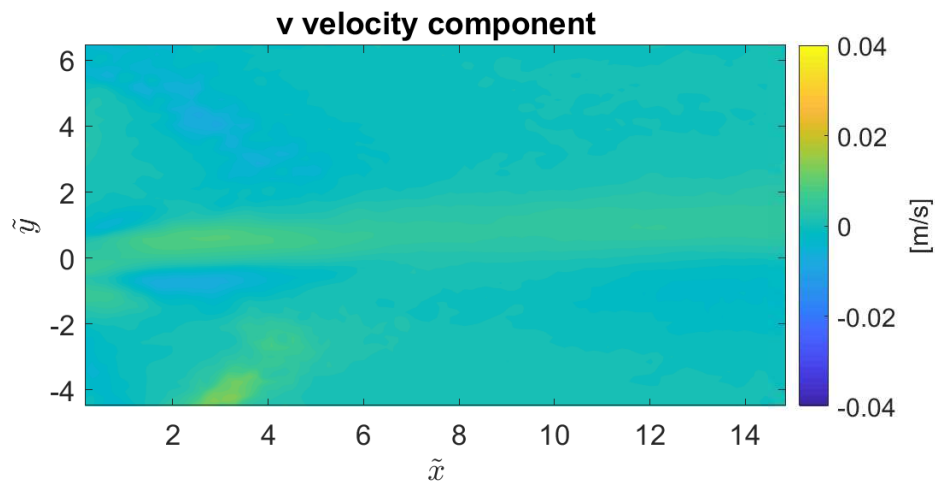


Figure 4.4: Free jet velocity v component

Another interesting result is the vorticity field. In Figure 4.5 it is represented for the free jet.

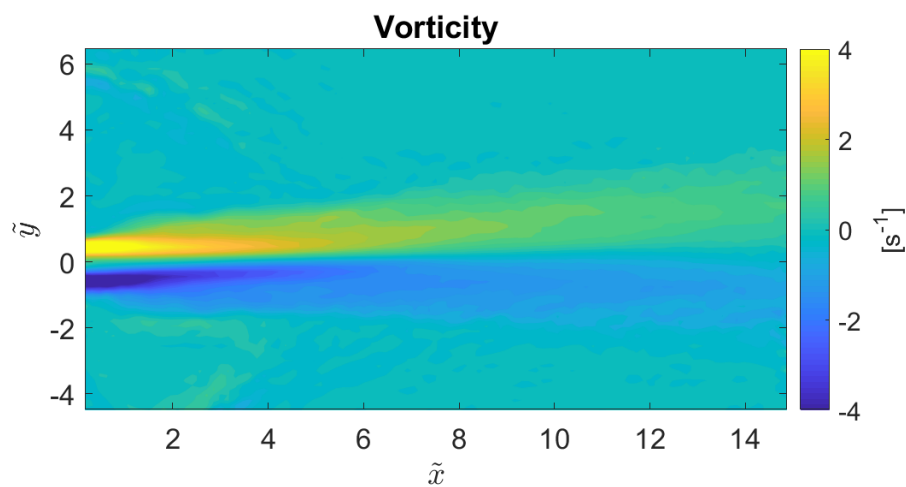


Figure 4.5: Free jet vorticity field

We can observe the symmetrical vorticity in the jet. In one side we have a vorticity in a positive sense while in the other side we have a vorticity of the same magnitude with opposite sense. Notwithstanding the fact that we can appreciate a slight deviation toward positive values of \tilde{y} that could

be produced due to some imperfection in the table, the result is that one expected.

It is important to have in mind that all the results are calculated as the mean vectors and not for a specific time. For that reason has no sense to calculate the velocity fluctuation as the average of the fluctuation is always zero. Nevertheless, it is interesting to calculate the Reynolds stress (see Figure 4.6).

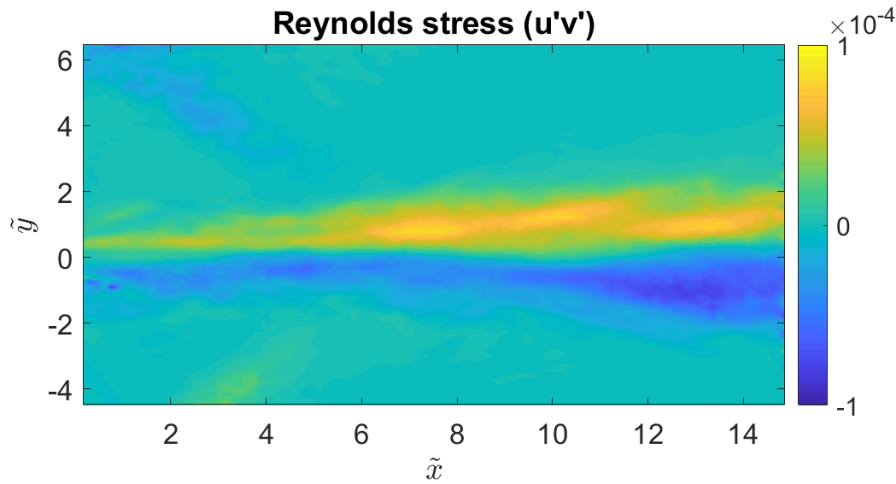


Figure 4.6: Free jet Reynolds stress distribution

The Reynolds stress is defined as the component of the Reynolds tensor (total stress tensor in a fluid) to value the turbulent fluctuations ($u'v'$) in fluids. We can expect that we will have a dominant component of u and then a component v that change the sign at each jet side. For that reason, we have positive values on one side and negative on the other. The values are with a magnitude order of 10^{-5} that indicates that the fluctuation in the v component is so small in comparison to the fluctuation in u component.

Then it is interesting to calculate the values of the statistical moments of order two, three and four, known as variance, skewness and kurtosis or flatness respectively.

The standard deviation can be defined as the root of the variance and gives information about the distance with respect to the average that has a velocity value. It can be calculated for each velocity component and can be expressed

as:

$$\sigma = \sqrt{\frac{\sum_{i=1}^N (\bar{x} - x)^2}{N}} \quad (4.3)$$

We can represent it for u and v components as shown in Figure 4.7 and Figure 4.8.

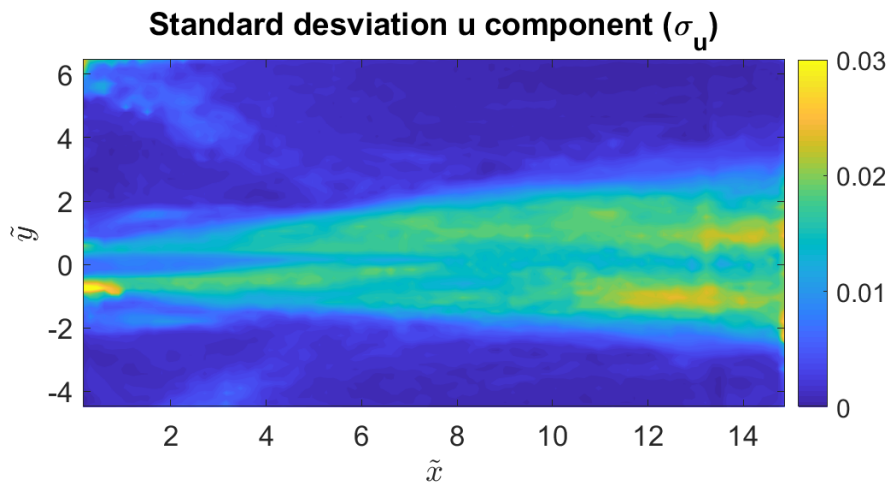


Figure 4.7: Free jet u component standard deviation

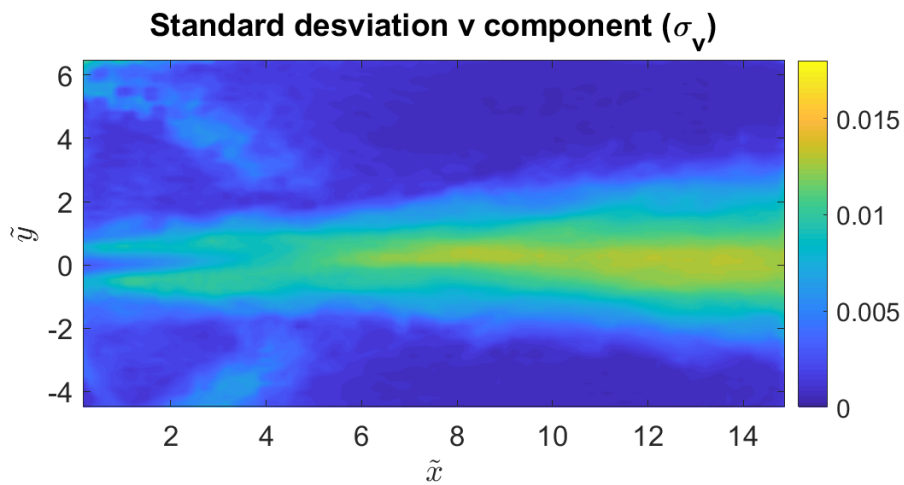


Figure 4.8: Free jet v component standard deviation

We can highlight that the jet shows the largest deviation except at the outlet that the deviation is near zero for the channel width and it decreases the width until at a point where you can't find the deviation absence. This is produced for an adimensional x length (\tilde{x}) of approximately 5.

The skewness gives information about the PDF (Probability Density Function) symmetry. If the PDF is symmetric, the asymmetry has a value of 0. A positive value means that we have a left asymmetry with respect to the average, while a negative value means a right asymmetry with respect to the average.

The skewness can be expressed as:

$$s = \frac{1}{N} \frac{\sum_{i=1}^N (\bar{x} - x)^3}{\sigma^3} \quad (4.4)$$

Representing it for u and v components we obtain the Figure 4.9 and Figure 4.10.

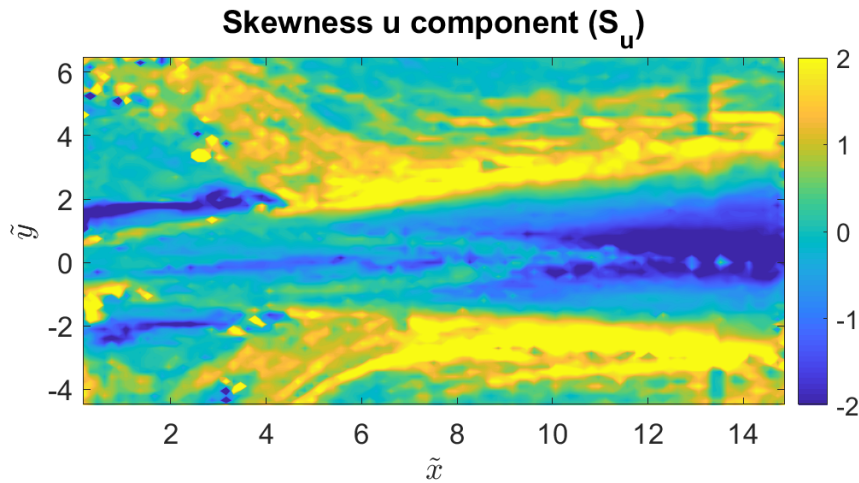


Figure 4.9: Free jet u component skewness

In this representation of u component, we can observe the effect due to the fact that we work in a finite surface. The skewness, in general, is more sensitive to the noise and small effects. We can observe that while in the jet borders we have a positive asymmetry in the centre we have the negative one. That happens up to $\tilde{x} = 4$ before, we can observe that the border has

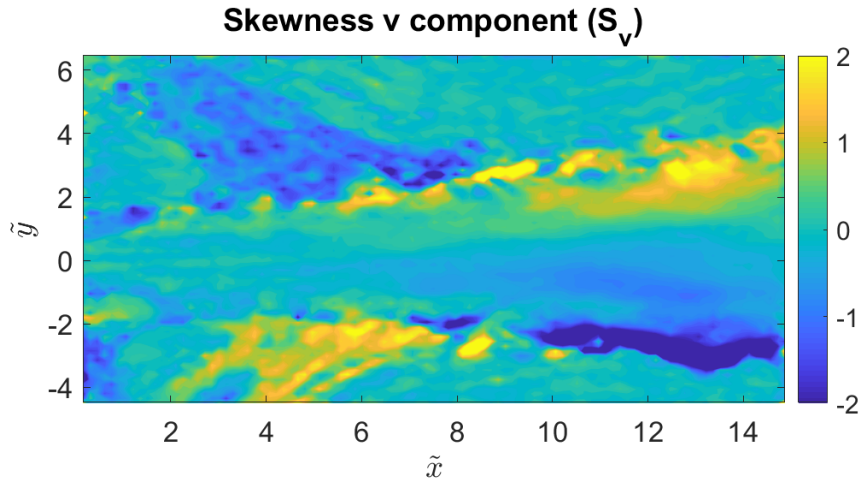


Figure 4.10: Free jet v component skewness

a negative asymmetry while the jet centre is practically symmetrical, as we can expect from the theory.

The analysis of v component shows that the asymmetries are compensated. We can expect this in order to obtain a straight jet.

The flatness factor gives information about the *flatness* of the PDF. A large value means that the tails of the distribution are large respect to the standard deviation. A small value means analogously small tails of the distribution.

The flatness factor can be expressed as:

$$K = \frac{1}{N} \frac{\sum_{i=1}^N (\bar{x} - x)^4}{\sigma^4} \quad (4.5)$$

In Figure 4.11 and Figure 4.12 is represented the flatness factor for u and v components.

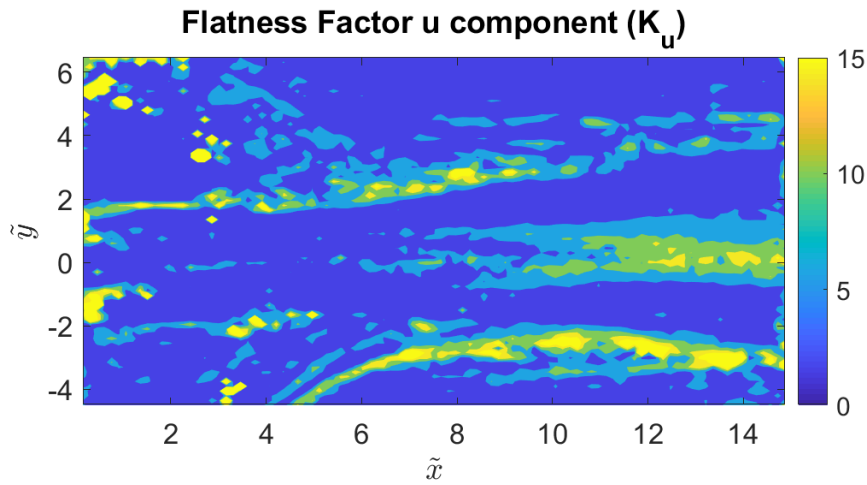


Figure 4.11: Free jet u component flatness factor

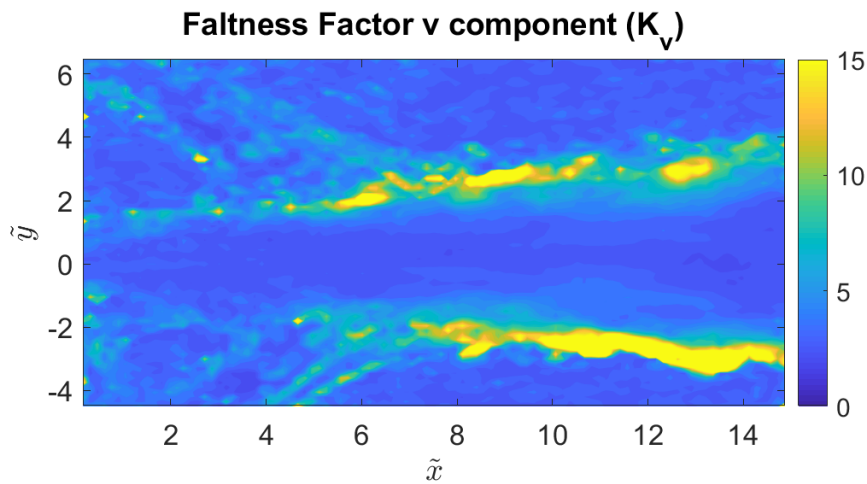


Figure 4.12: Free jet v component flatness factor

In this analysis, we can identify also some noise but it is possible to appreciate for u component that the inner part of the jet has a value near 0 until $\tilde{x} = 8$ while the borders have high values.

Respect to the v component the inner part of the jet is more uniform and are the borders that always have the high kurtosis values.

We can take transversal sections in the vector field in order to extract some

relevant information. In our case, it is selected to see the velocity, vorticity and Reynolds tensor profiles.

In the first case, it is extracted the velocity u component data at different distances of the outlet. Adimensionalizing respect to the maximum velocity (U_c) at each distance we obtain the profiles represented in Figure 4.13.

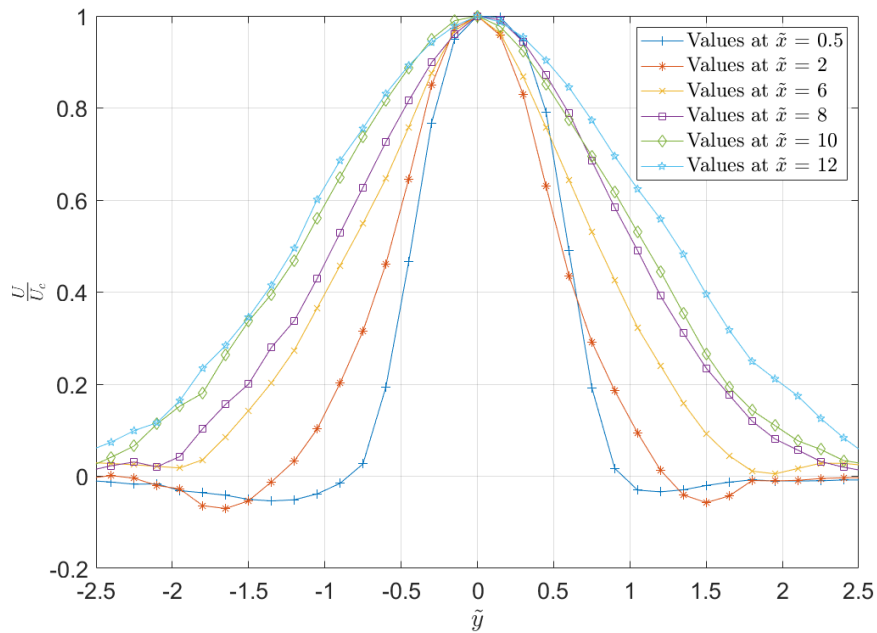


Figure 4.13: Free jet velocity u component profiles

As we can see the result is symmetrical with respect to the axis that crosses the zero. For the values near to the outlet, we can see the effect of the recirculating created around the boxes, that is why we observe that negative values. As commented in the Introduction, the transversal length of the jet increases as it passes along the tank. This is possible to observe in the different profiles as the profile at $\tilde{x} = 12$ has the maximum size while the one at a value 0.5 has the minimum.

We could expect that the profile at small values is similar to the turbulent outlet profile. Nevertheless, we can see that it does not coincide at all (see Figure 4.14). This could mean that the jet it is not completely developed and therefore, it is not completely turbulent. This can be solved by putting more spikes in the channel in order to force more the transition.

Then in figure 4.15, it is represented the vorticity profile at the same different

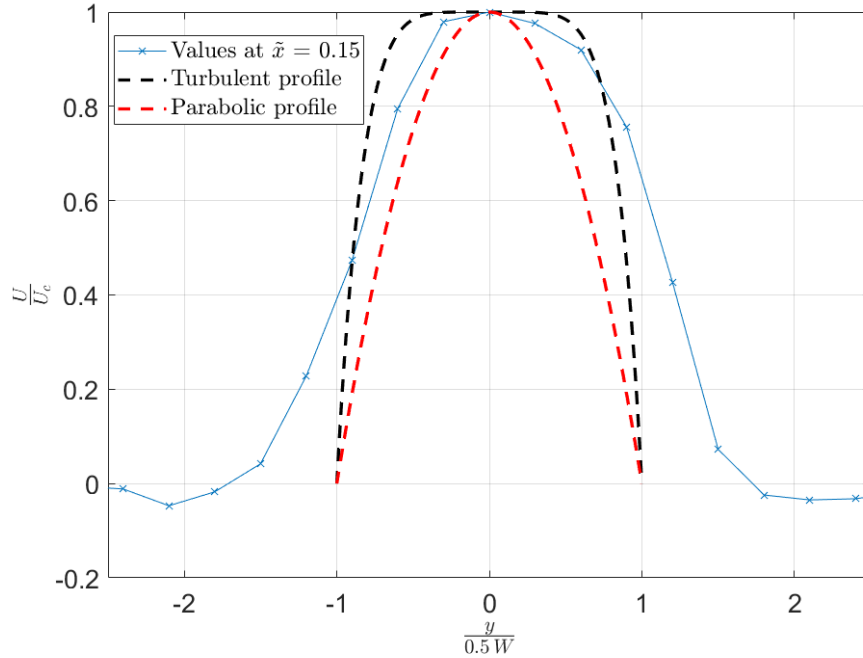


Figure 4.14: Free jet velocity u component profile at the outlet

distances.

In this plot, we can observe that exist symmetry respect the point $(0,0)$. It means that the jet centre has no vorticity and the vorticity at sides is equal with different signs. Besides at the lateral limits the vorticity is again zero as the jet perturbation is practically negligible. This is a characteristic vorticity distribution in a free jet. We can observe a slight deviation of the null vorticity point towards positive values of \tilde{y} , this means that the jet tends to deviate. This could be produced by some element that disturbs lightly the jet direction. In any case is a negligible deviation that will not have a relevant repercussion in the later study.

Finally, in Figure 4.16 it is represented The Reynolds tensor profiles.

We can note that also in this case there is symmetry respect the origin point. This is because the jet centre has only the horizontal component, so the fluctuation in the v component is null, while the rest of the points have a v component what serves to widen the jet. At the extremes is near zero due to is the not perturbed zone and the fluctuation in both components has no relevance.

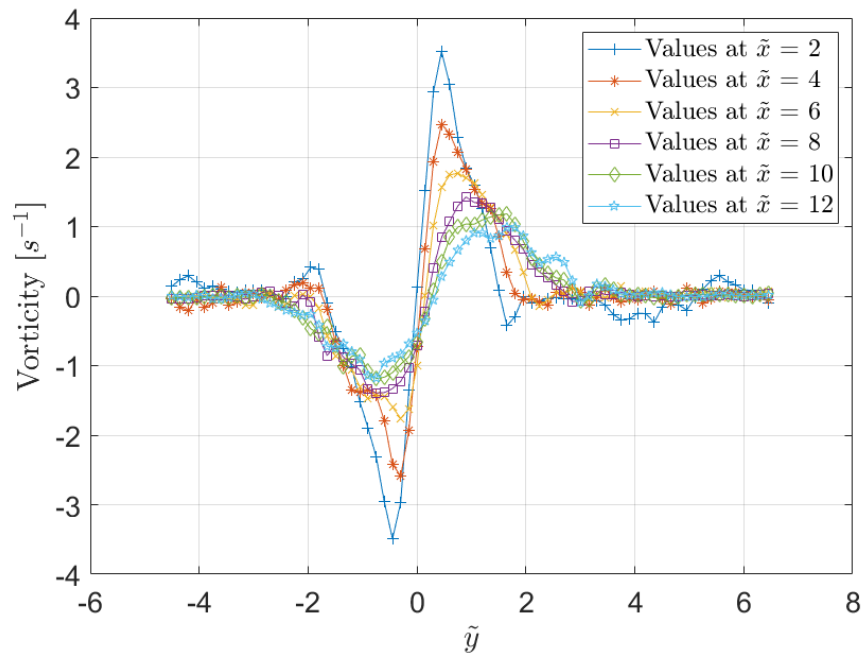


Figure 4.15: Free jet vorticity profiles

Also, it is important to compare the results with the available literature. In Figures 4.17, 4.18, 4.19 and 4.20 it is represented some free jet experiment results of various authors. We can notice that the results are similar to the results obtained in this work.

In general, after realizing the complete free jet analysis we can conclude that the results are acceptable and it is possible to carry out a good Coanda jet study. We should have in mind that the free jet configuration it is difficult to establish as any small factor could impact in its undisturbed condition.

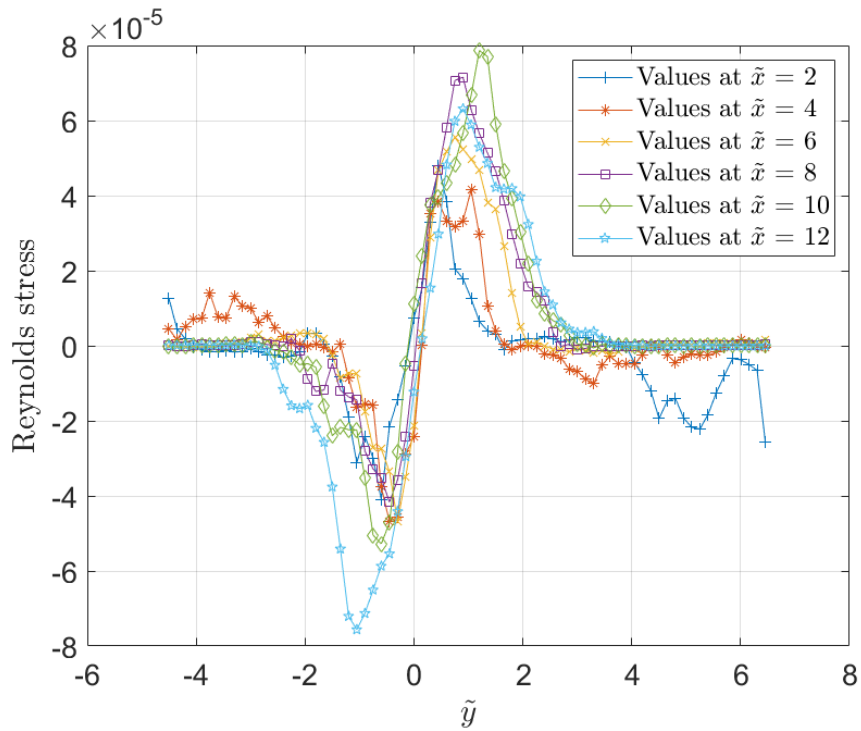


Figure 4.16: Free jet Reynolds tensor profiles

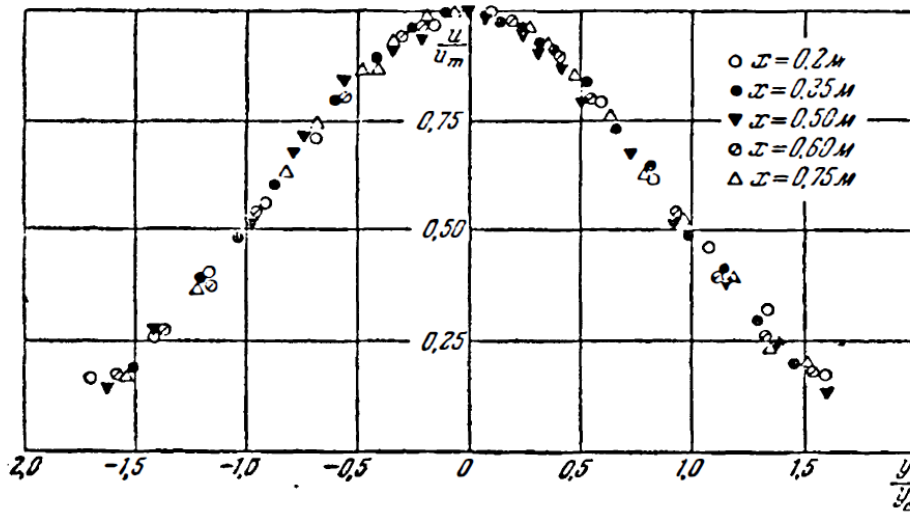


Figure 4.17: Free jet dimensionless velocity profile (Abramovich et al., 1984)

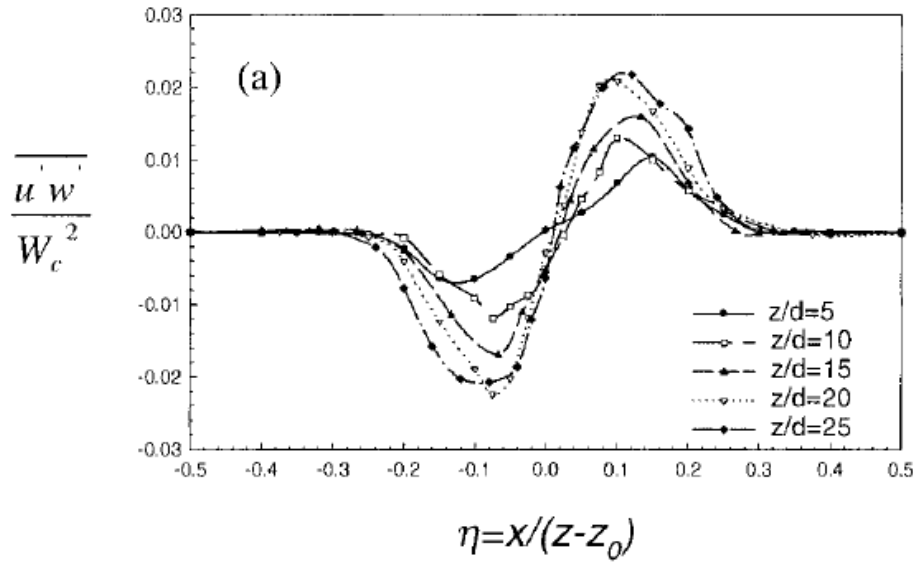


Figure 4.18: Free jet reynolds stress profile (Kuang et al., 2001)

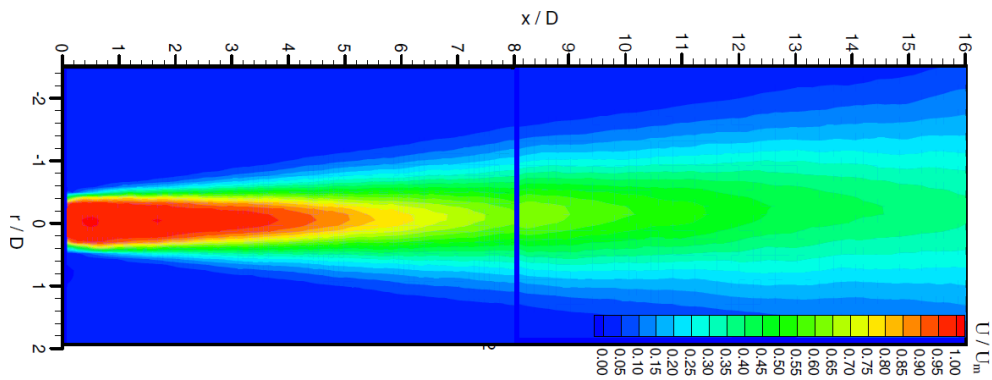


Figure 4.19: Free jet velocity PIV results (Mi et al., 2007)

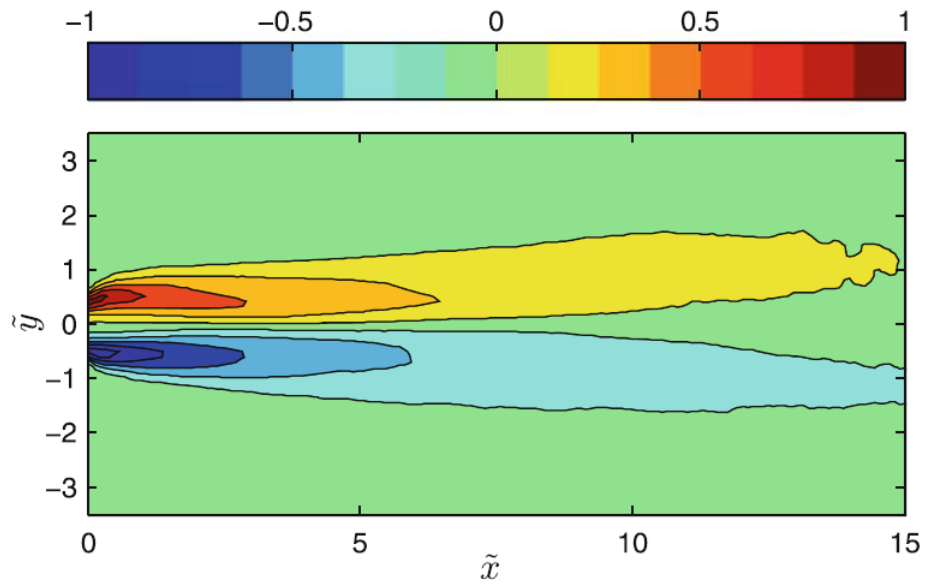


Figure 4.20: Free jet vorticity PIV results (Miozzi et al., 2010)

Chapter 5

Coanda Jet experience

In this chapter, the Coanda jet experience will be studied. In particular, the variation of the reattachment point when varying the wall distance. The results will be also compared with those obtained in the previous chapter in order to understand better the effect.

5.1 Configuration

As we want to do the study with the same Reynolds and Froude numbers than the free jet experience, the values of the flow rate and water level will be the same than the calculated in section 4.1.

The difference between both configurations is that in this one there is a new parameter to be taken into account, namely, the wall distance to the output (\tilde{H}). In particular there will be three different configurations in order to set the wall at $\tilde{H} = 3$, $\tilde{H} = 4$, $\tilde{H} = 5$.

It is important to consider that our measurement area is 70 cm long so the effects produced at a major distance will not be possible to analyze.

Also, the camera will be relocated for this measures moving it about 10 cm to the wall placed side. The jet will not be symmetrical anymore and with the initial configuration, it is not possible to see the wall reattachment for greater distances of $\tilde{H} = 4$.

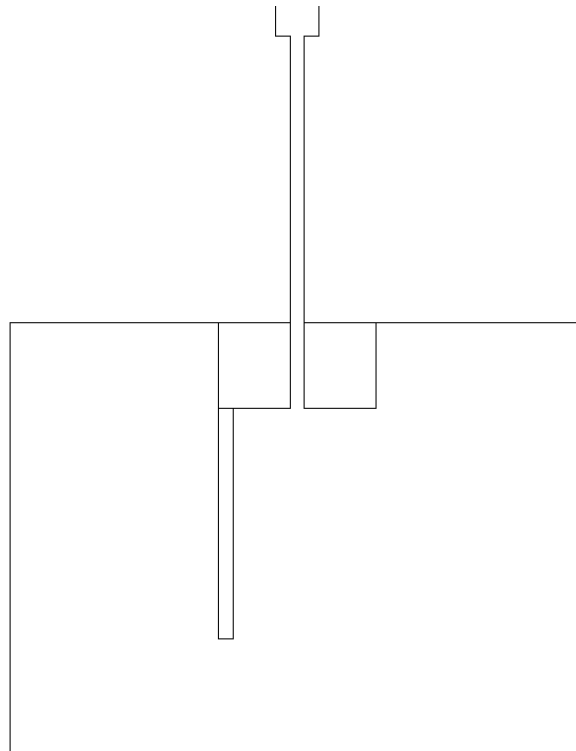


Figure 5.1: Table configuration for Coanda jet

5.2 Results

Vector field

As in the previous chapter, after doing the analysis we will obtain a vector field. In this case, we obtain three vector fields, one for each wall distance studied.

In figure 5.2 there is represented the different vector fields for the Coanda jet. In these images, we can appreciate the variation of the reattachment point, which will be studied in more detail later on.

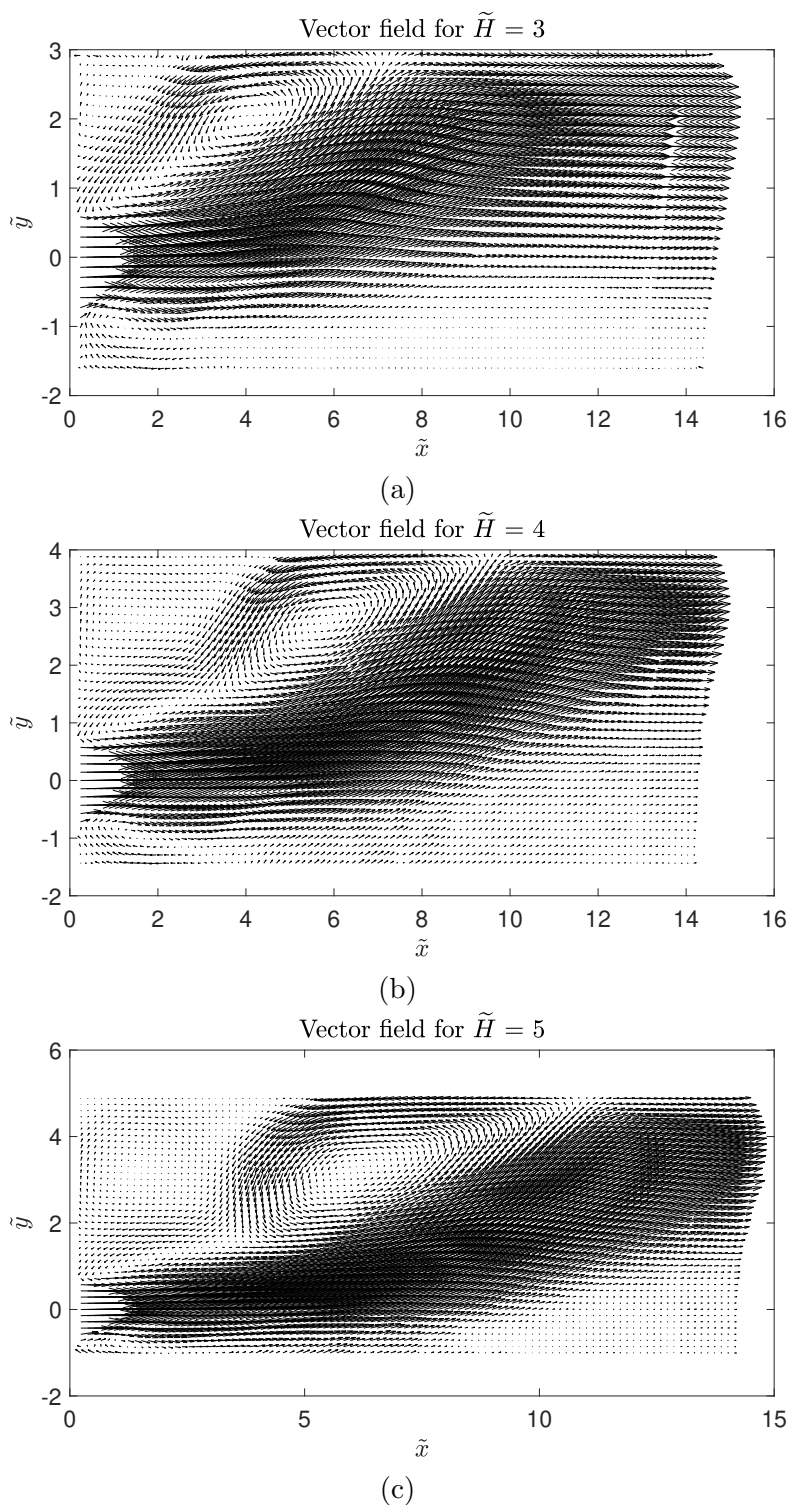


Figure 5.2: Coanda jet vector field

Also, we can see that the vector density is large enough to obtain valid results. If we pay attention it is possible to observe one anomaly in the values near $\tilde{x} = 13$. This effect is due to the joint line created during the assembly phase. It could be reduced by doing some preprocessing actions, but the best solution is to change the table surface in order to remove that line. Regrettably, as the time to realize the experiment is short and that solution implies too much time to fix, it was decided to let it as it was since it does not affect to the relevant zones of the experiment.

Velocity components

In Figure 5.3 there are represented u component velocity of the different configurations with the streamlines. Plotting the streamlines it is clearly visible the recirculating zone before the reattachment point. In particular, it is possible to see that two counterrotating vortices increase in size as the distance from the wall increases.

About the values of u component, we can see that are the same than in the free jet. It is something obvious as we set the same Reynolds conditions.

If we focus on the wall we can have the first approximation of the reattachment point. In Figure 5.3 (a) we can identify that the point where the recirculating finish is near $\tilde{x} = 7$. In Figure 5.3 (b) that point is less than $\tilde{x} = 9$ while in Figure 5.3 (c) the point moves to a value slightly greater than $\tilde{x} = 10$.

This serves for having a first magnitude order but it is not a rigorous definition. So these values are used to see, immediately after taking the images, if the results could be valid or not. In our case, we can appreciate that the values are similar to those ones calculated using (1.1), so we can conclude that our measures are well done and we can analyze them.

Regarding the v component, in comparison with the free jet, there are relevant values. We can observe in Figure 5.4 that there is a positive zone, the yellow one, that tends to go towards the wall. These positive values expand along \tilde{x} the greater the distance from the wall. We can observe in Figure 5.4 (a) that the positive values arrive at $\tilde{x} = 8$ while, in Figure 5.4 (c), arrive until $\tilde{x} = 12$.

Additionally, we can detect a negative value zone in correspondence to the zone where the two recirculating vortices join. This serves to identify the size of the two vortices.

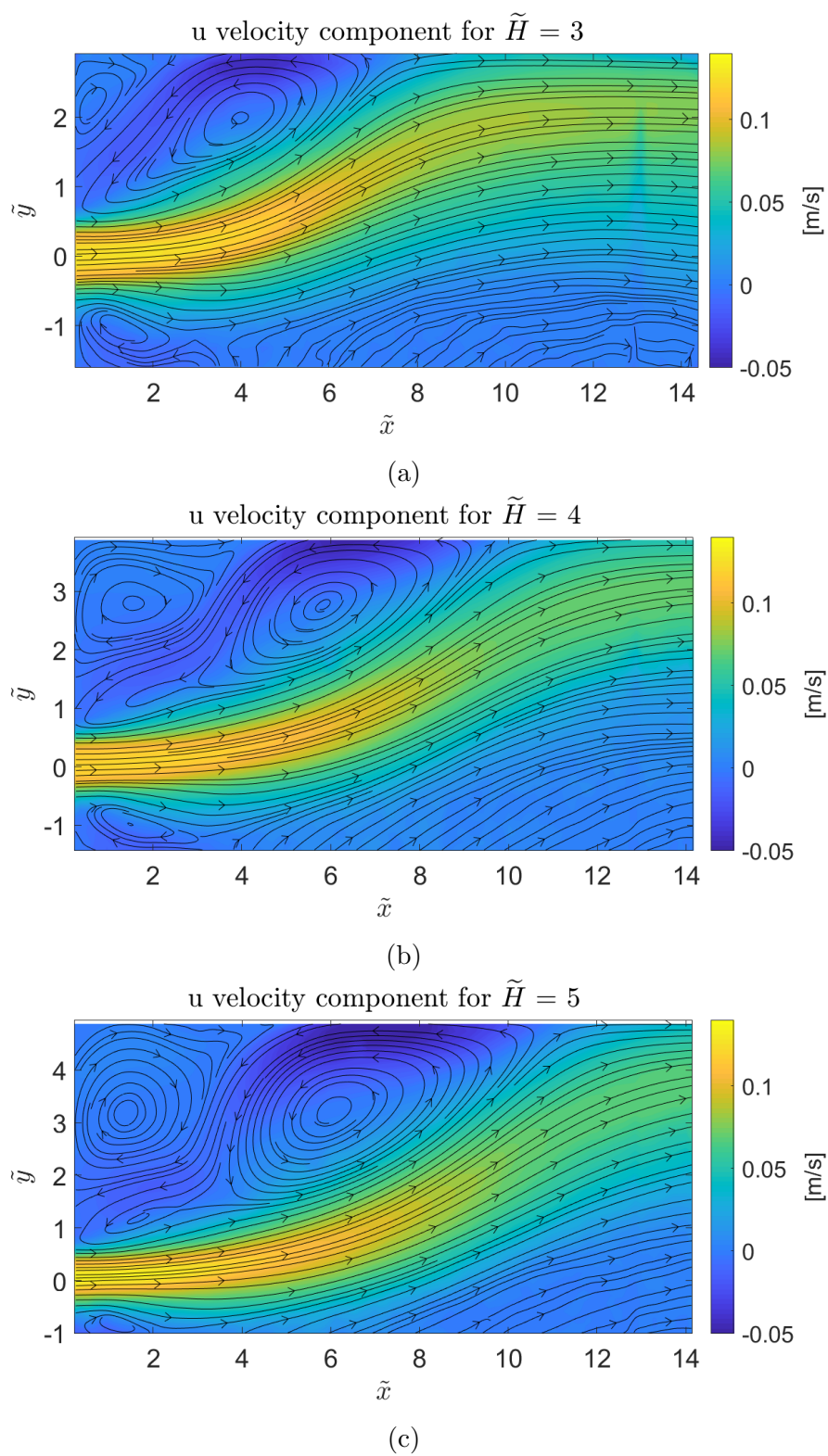
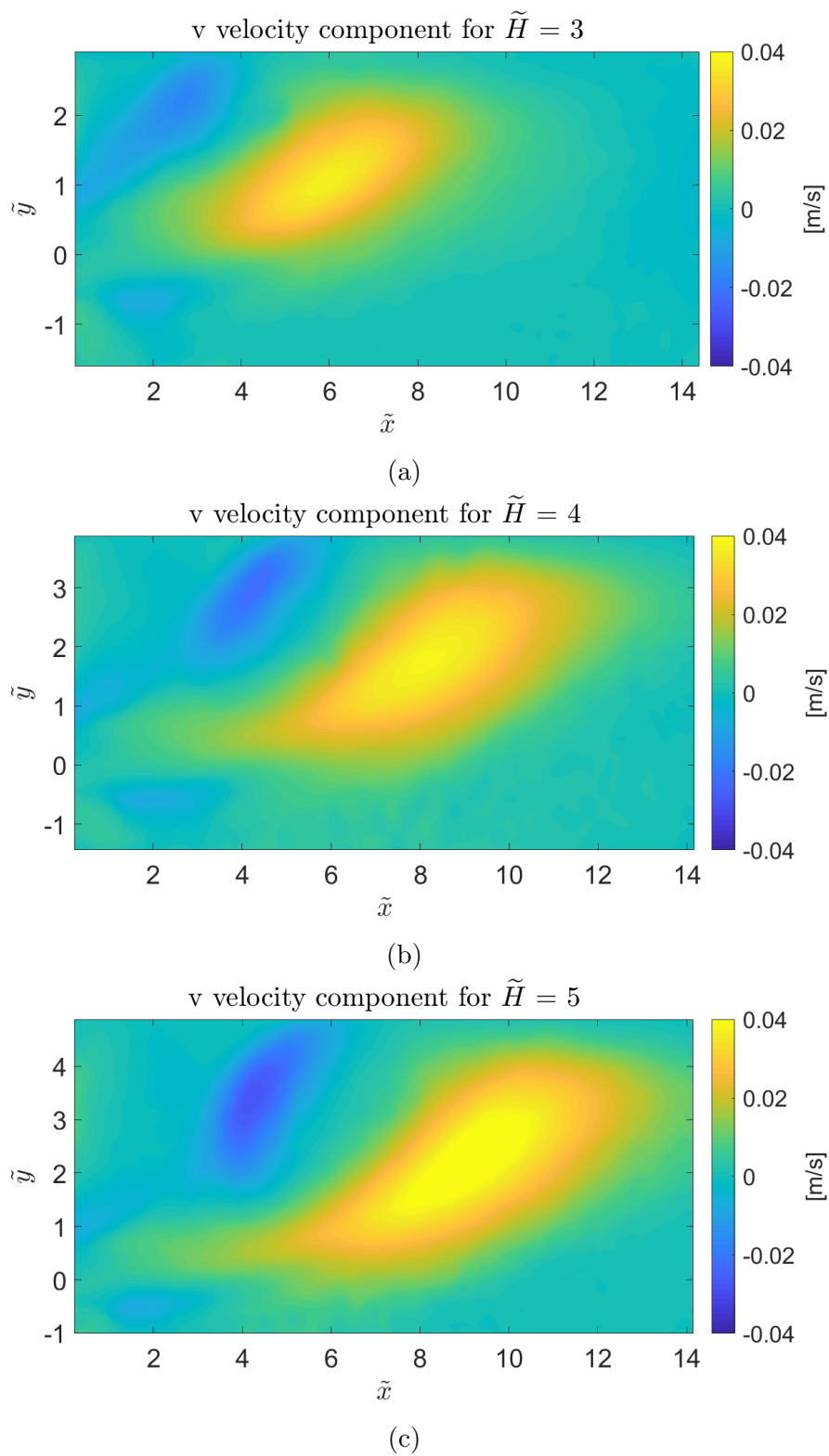


Figure 5.3: Coanda jet velocity u component

Figure 5.4: Coanda jet velocity v component

Vorticity

Then it is also interesting to study the vorticity field in each configuration (see Figure 5.5). We can note that the line with zero value deviates towards the wall and let us identify the jet centre. It is also remarkable that in the zone where the two recirculating zones join, there is the contrast between positive and negative vorticity values. Of course in this case, unlike the case of the free jet, there is no symmetry and it is not possible to affirm that positive and negative values are present to the same extent.

Reynolds stress

Later on it is possible to see the Reynolds stress distribution. In Figure 5.6 it is represented for the three different configurations.

We can observe that, in contrast to the free jet, there are now more values of the magnitude order of 10^{-4} that means that the fluctuation in the v component has gained more relevance.

Standard deviation

Also, it is possible to make a statistical study of this configuration. As in the case of the free jet, we can study the standard deviation, the skewness and the flatness factor of the Coanda jet. All of these factors are defined previously in section 4.2.

If we pay attention to the standard deviation of u component (Figure 5.7), we can detect the zone where the deviation is nearly null. Now it is no more straight but it arrives until, more or less, the same values of the free jet. For this results, it is not possible to identify an evolution of this zone for the different configurations. In Figure 5.7 (b) it is larger (arrive up to a value of $\tilde{x} = 6$) but, in Figure 5.7 (c), it is shorter arriving up to a value of $\tilde{x} = 4$.

For the standard deviation of the v component (Figure 5.8), we can observe that in general, the deviation is smaller than for u component. The null deviation zone at the jet output is, in this case, shorter than for u component. This happens also for the free jet configuration and means that the v component starts to fluctuate before u component.

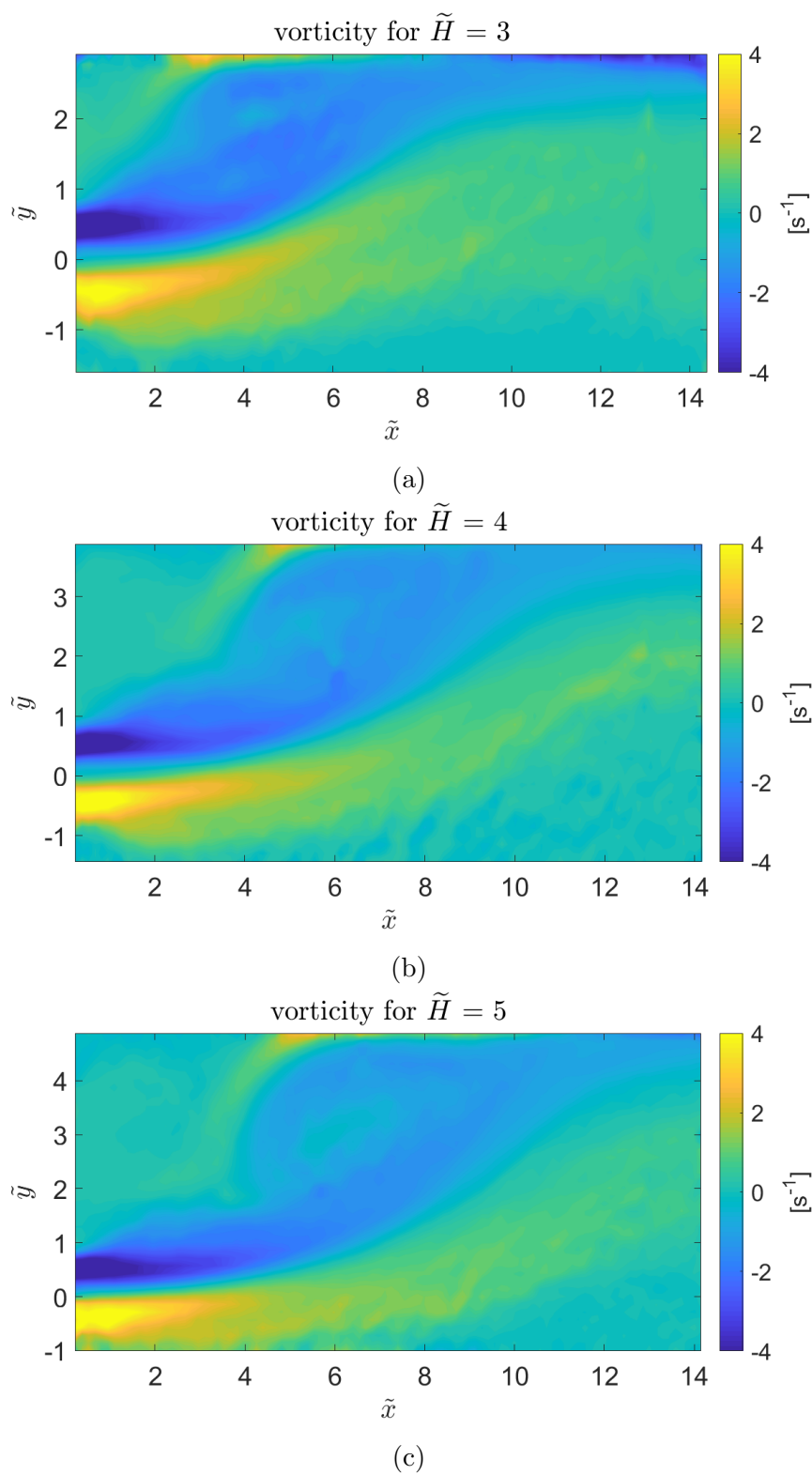


Figure 5.5: Coanda jet vorticity field

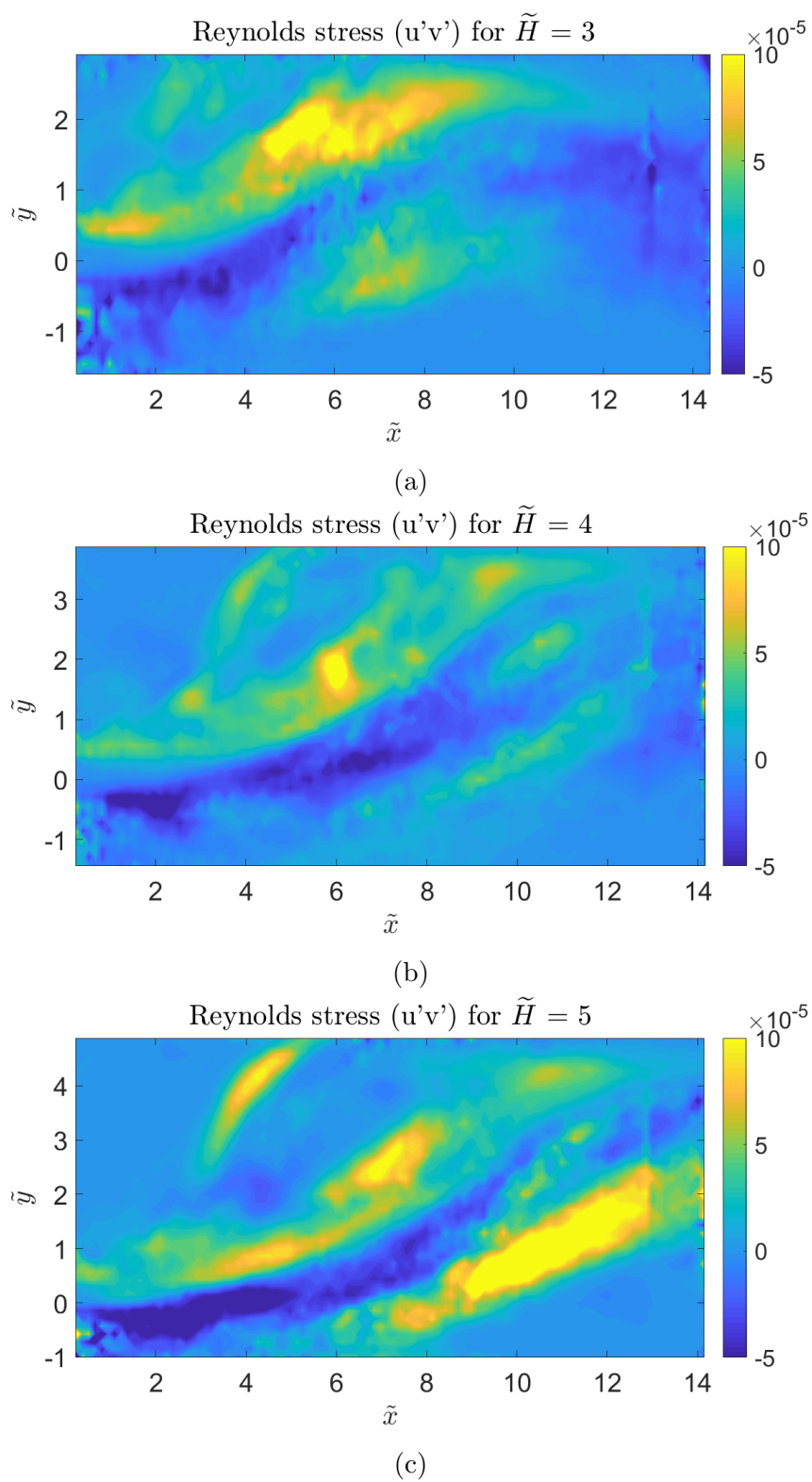
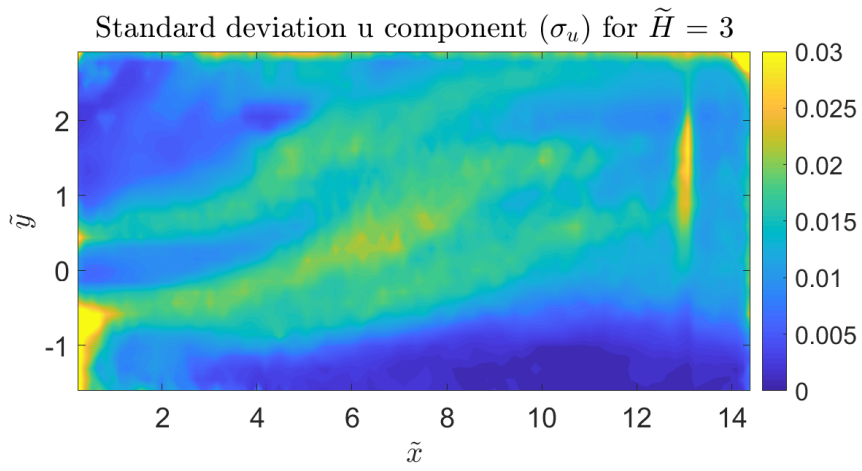
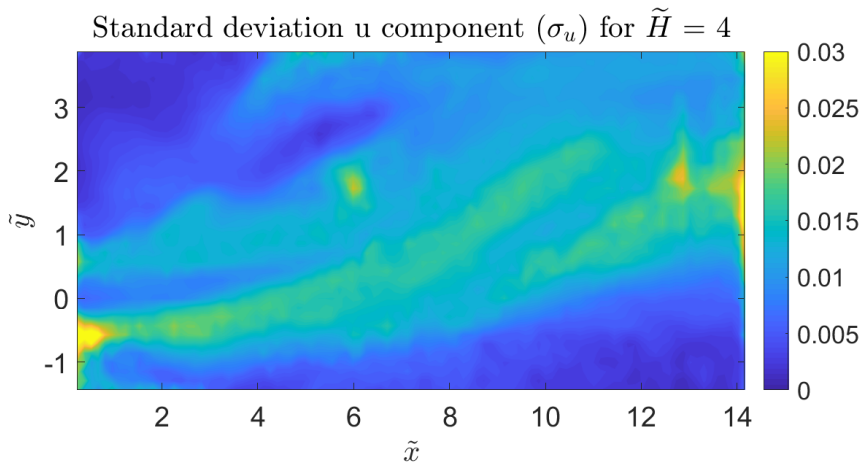


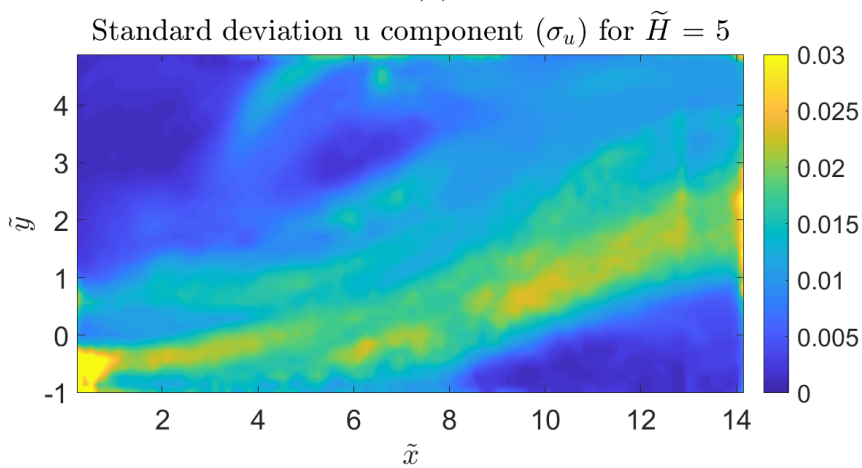
Figure 5.6: Coanda jet Reynolds tensor distribution



(a)

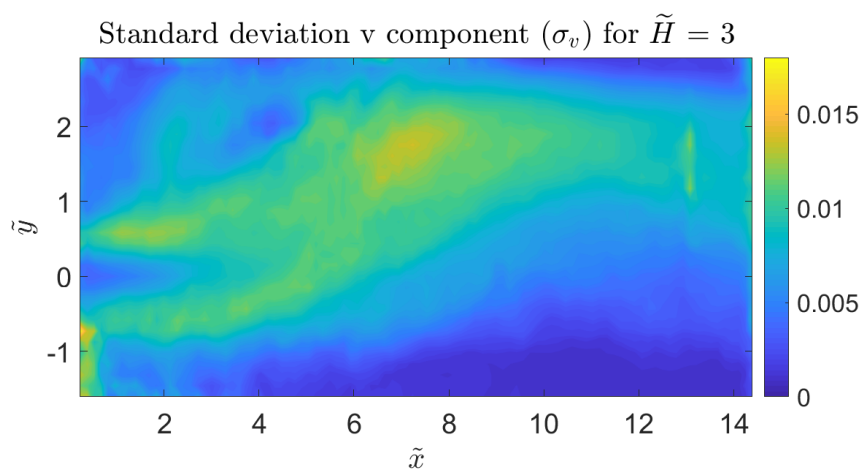


(b)

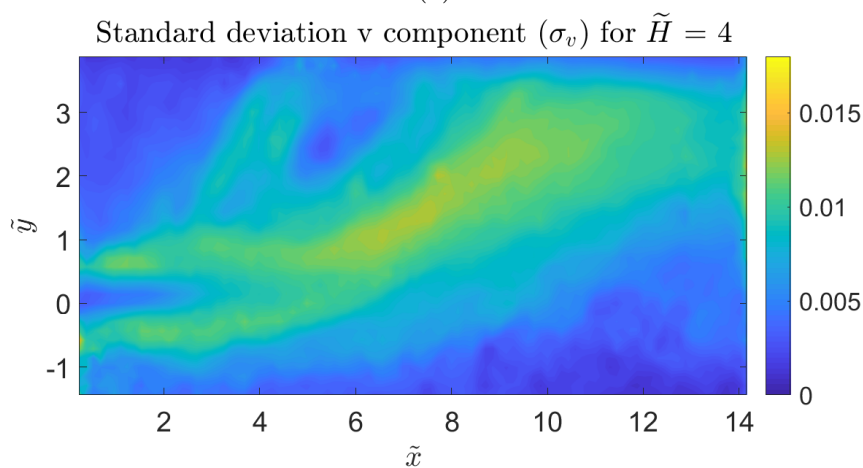


(c)

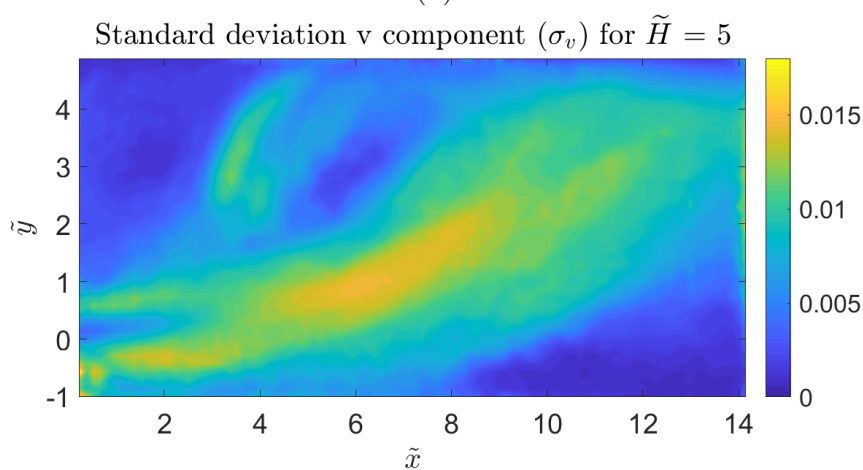
Figure 5.7: Coanda jet u component standard deviation



(a)



(b)



(c)

Figure 5.8: Coanda jet v component standard deviation

Skewness

The analysis of u component skewness is represented in Figure 5.9. We can observe that the closer the wall is, the greater the pressure gradient that pushes the jet towards the wall is. Therefore, we can see more skewness in Figure 5.9 (a) than in Figure 5.9 (b), where the jet moves smoother to the wall.

As in the free jet case, the inner part of the jet has negative skewness while the positive values are produced outside the jet limits.

In Figure 5.10 we can see the v component skewness distribution. In general, it is shown a more homogeneous field. Neglecting the noise produced in this analysis, in general, we could appreciate a negative skewness along the jet. This is similar to the result obtained for the free jet without the remark of the borders.

Flatness factor

Finally, the flatness factor is represented in Figure 5.9 and Figure 5.10. In comparison to the results of the free jet, we can see that the values are slightly higher. Besides, it can be noticed a slight increment of the values as the wall moves away from the output.

Velocity profiles

In this case, it is also possible to extract the information from the transversal sections. In figure 5.13 it is showed the information of the u component velocity.

As previously commented, there is no more symmetry, so, the peaks of the curves are displaced to the right side. It can be noticed that for the values of $\tilde{H} = 3$, the first peaks expand more between them than for greater distances of \tilde{H} . This is due to the fact that the pressure gradient is more accentuated for the configurations where the wall is near. In fact, for large distances, where the jet is completely reattached and adapted the peak distances are so small.

In fact in Figure 5.14 and Figure 5.15 it is possible to see that the first peaks are closer, as the pressure gradient is weaker.

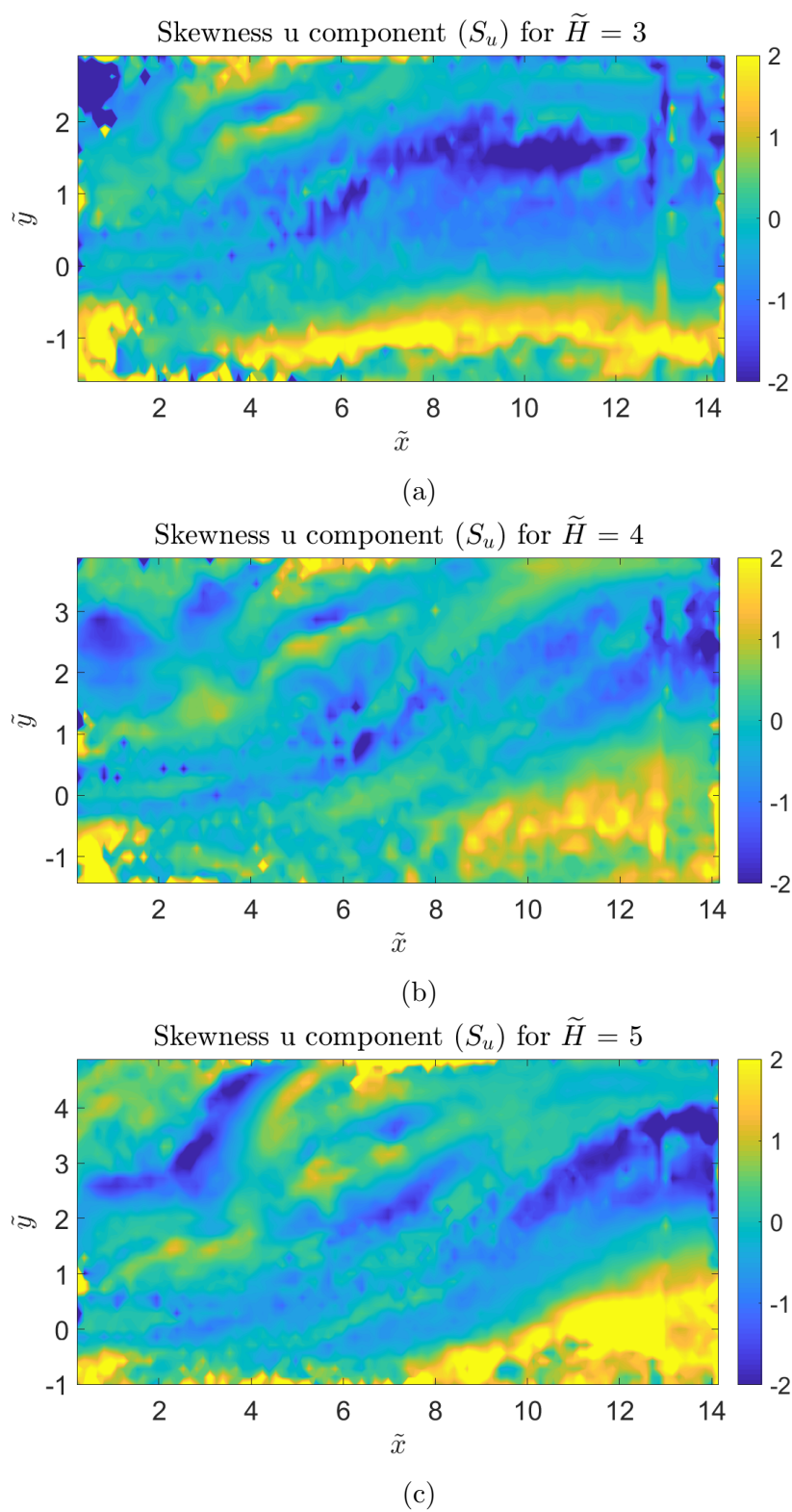


Figure 5.9: Coanda jet u component skewness

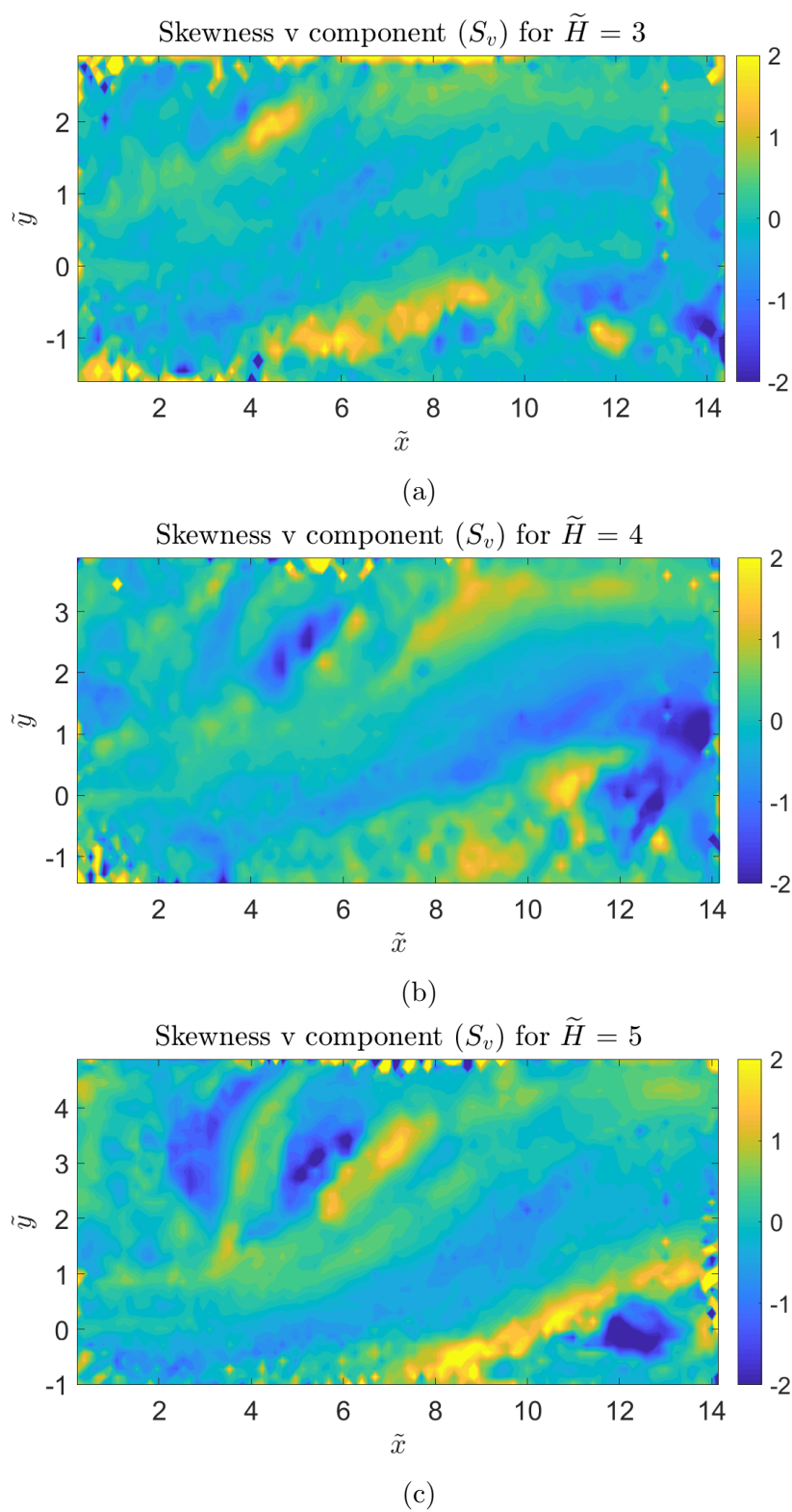
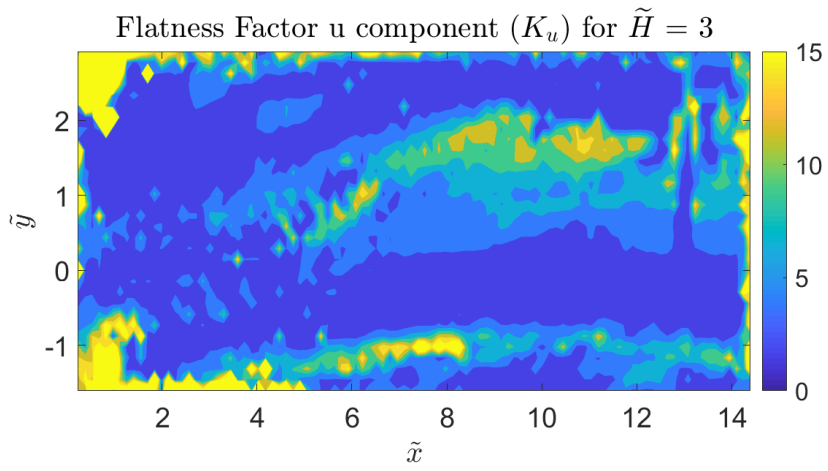
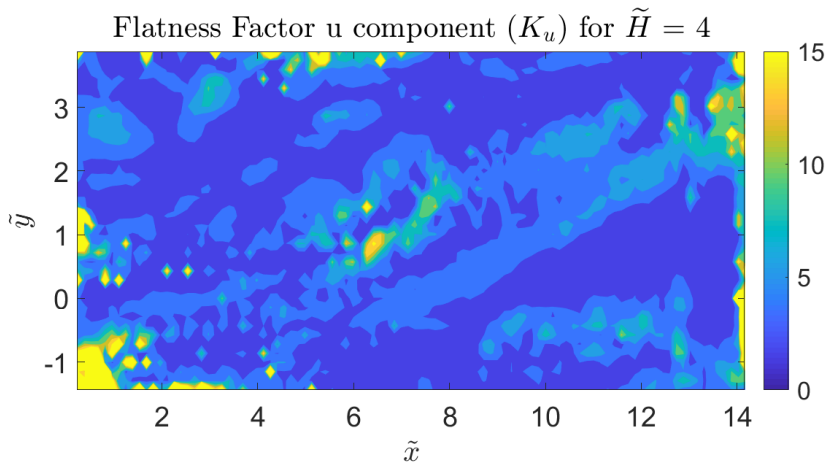


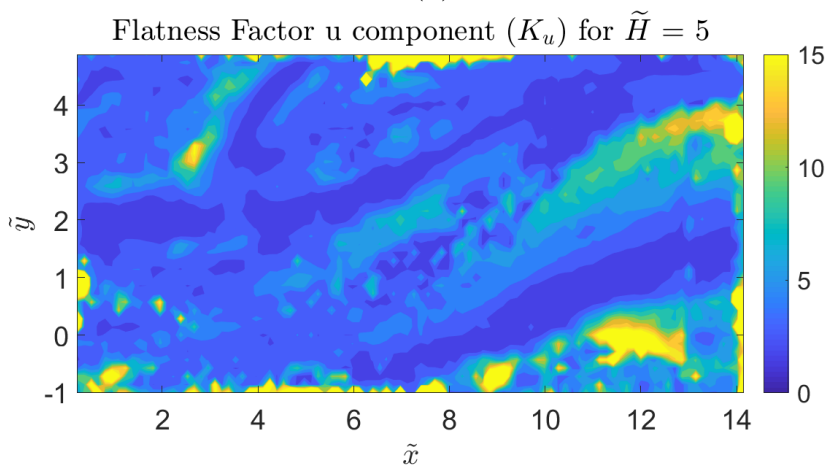
Figure 5.10: Coanda jet v component skewness



(a)



(b)



(c)

Figure 5.11: Coanda jet u component flatness factor

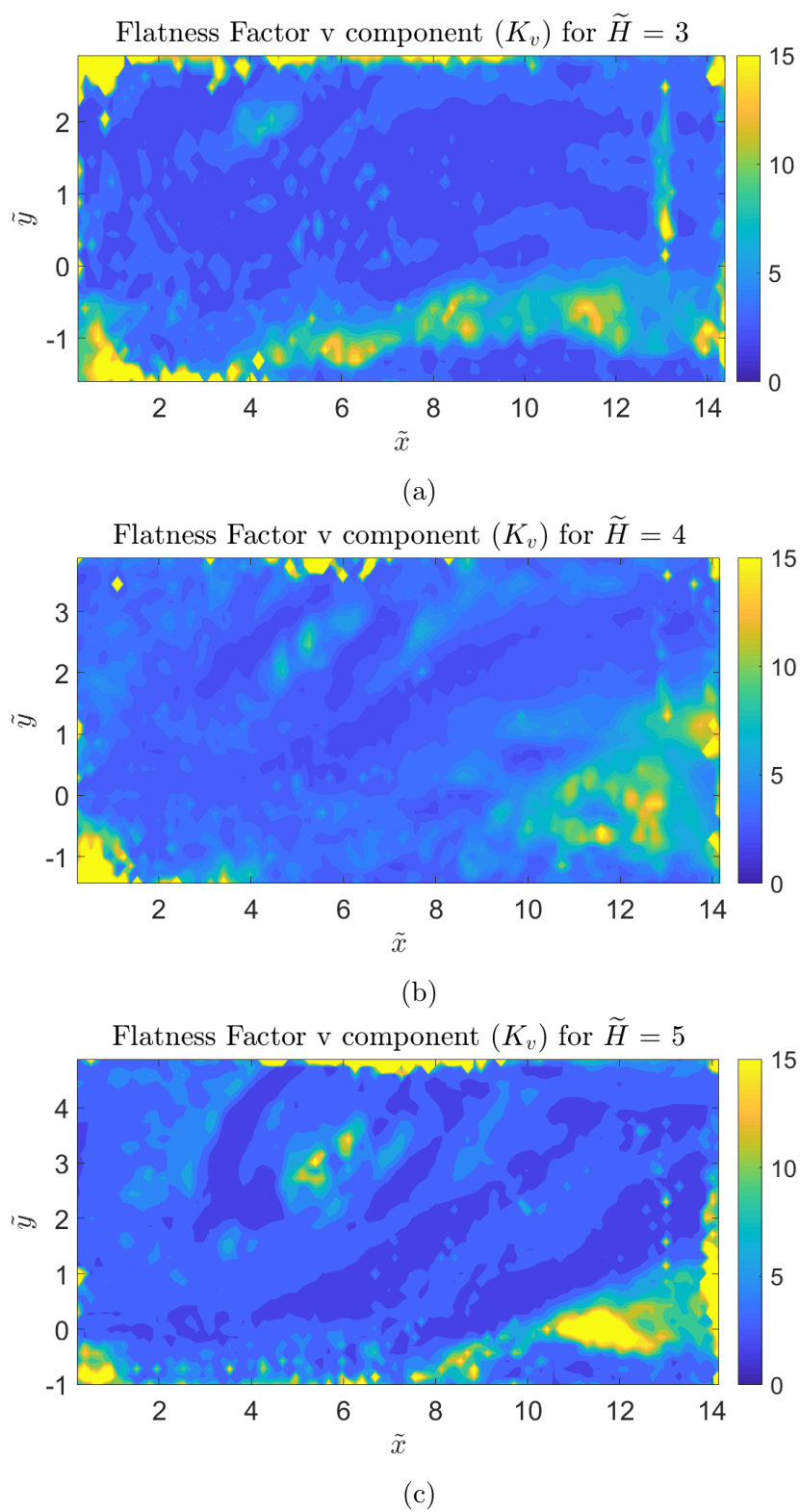


Figure 5.12: Coanda jet v component flatness factor

Another interesting analysis is the observation of the negative values, which means the so called recirculating zones. For the first configuration (Figure 5.13), we can see that curves up to $\tilde{x} = 6$ present values under zero. That means that the reattachment will be between $\tilde{x} = 6$ and $\tilde{x} = 8$. Analogously, for the other configurations, we identify that the reattachment is produced at a value greater than $\tilde{x} = 8$ and $\tilde{x} = 10$ respectively.

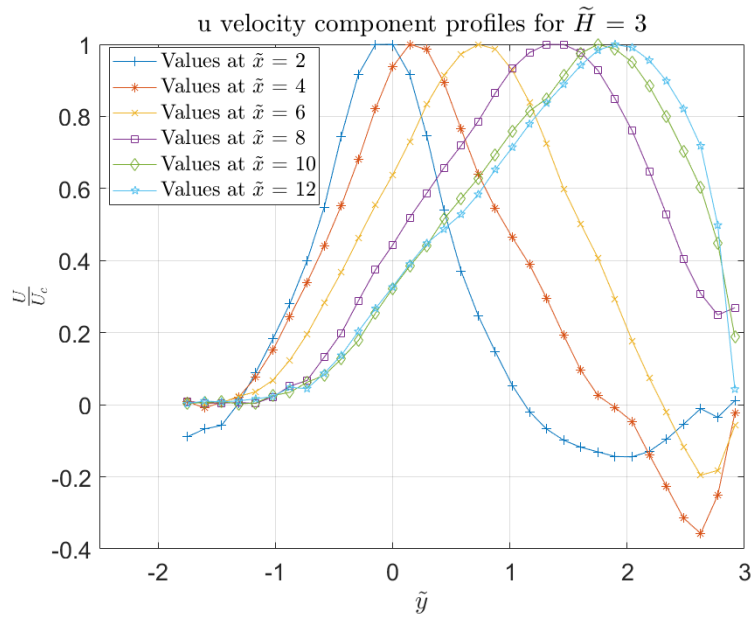


Figure 5.13: Coanda jet velocity u component profiles for $\tilde{H} = 3$

Vorticity profiles

Then it is represented the vorticity profiles for the different wall distances (see Figures 5.16, 5.17 and 5.18). With this plots, it is checked that effectively, the null vorticity line deviates towards the wall, as it was detected in the vorticity field.

The values near the wall can't be considered as acceptable. The PIV technique shows some problems to represent the real behaviour in the wall. For that reason, it is no possible to interpret the vorticity at the maximum \tilde{y} values.

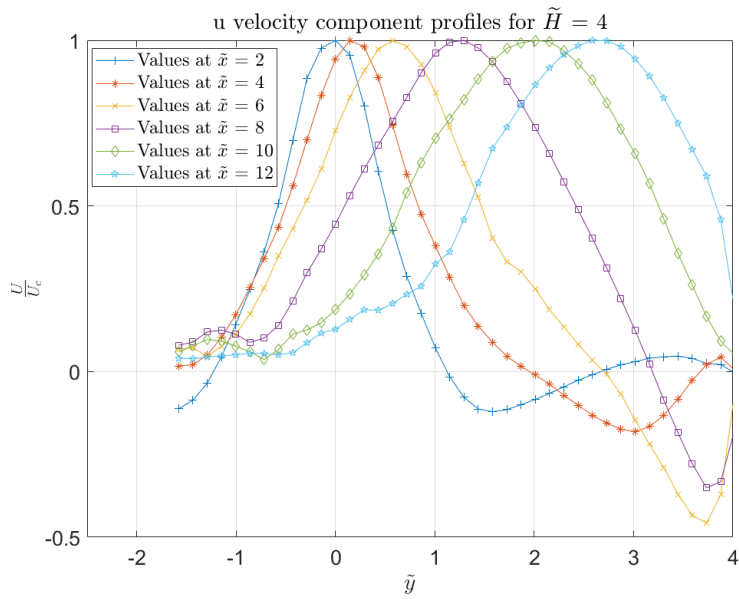


Figure 5.14: Coanda jet velocity u component profiles for $\tilde{H} = 4$

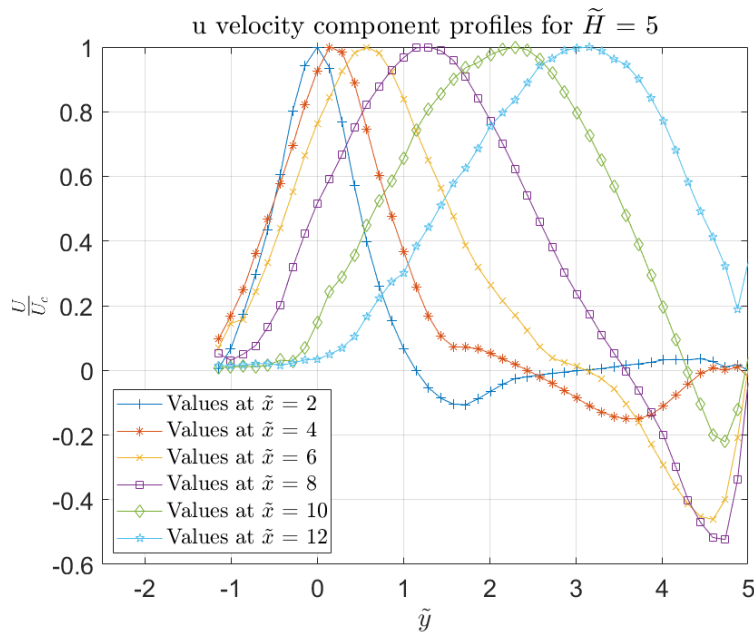
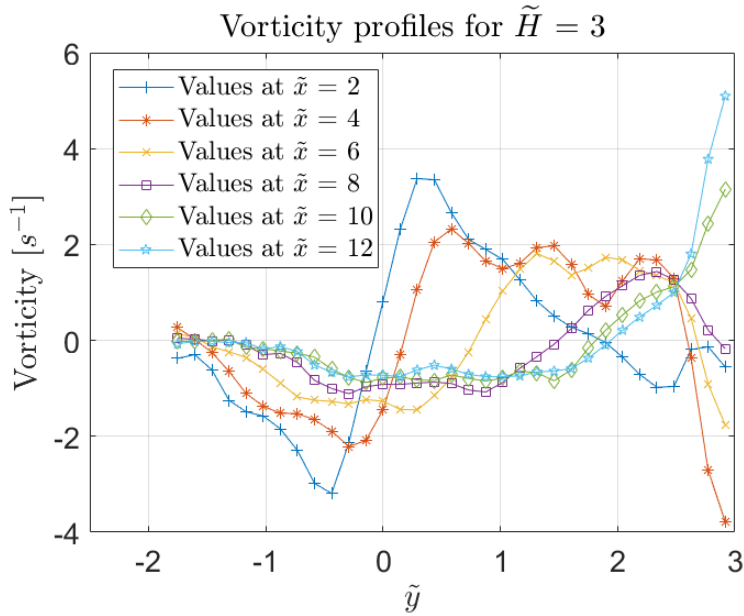


Figure 5.15: Coanda jet velocity u component profiles for $\tilde{H} = 5$

Figure 5.16: Coanda jet vorticity profiles for $\tilde{H} = 3$

Reynolds stress profiles

Finally, the Reynolds stress profiles are represented in Figures 5.19, 5.20 and 5.21.

The first observation that we can make is that the values increase as \tilde{H} does. In general, it presents values greater than the obtained in the free jet. Besides, the values tend to go to zero as in the wall the fluctuation should be null.

In every plot, we can find a peak that is clearly greater than the others. This could be produced by some noise in the results. Additionally, it is observable that the positive values are in general greater than the negative values, this means that in general, the fluctuation is produced for positive values of v in order to deviate the jet towards the wall.

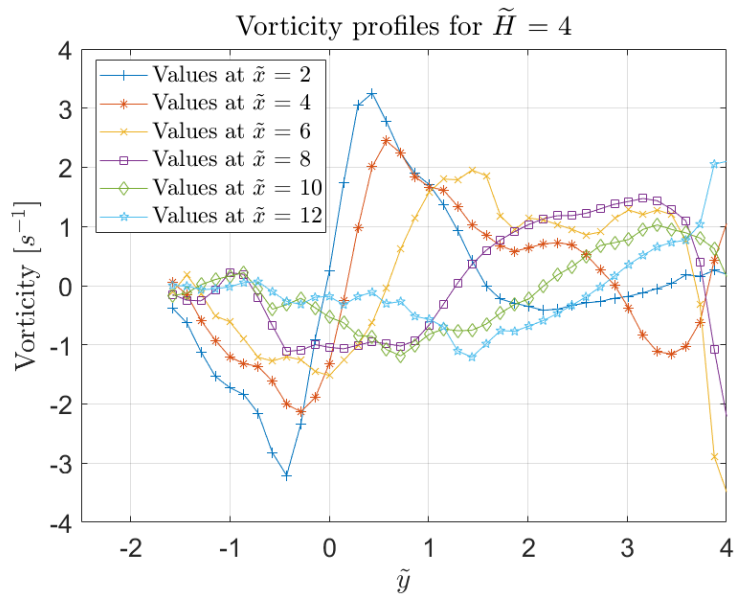


Figure 5.17: Coanda jet vorticity profiles for $\tilde{H} = 4$

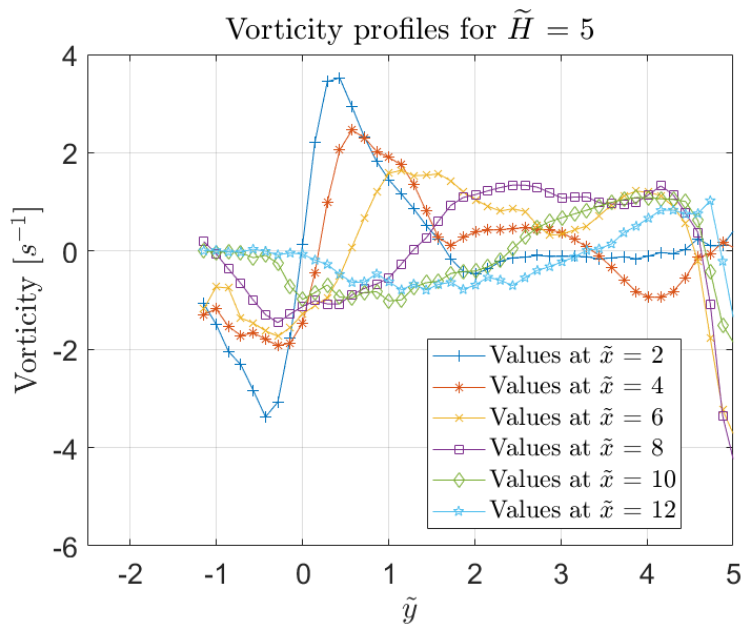


Figure 5.18: Coanda jet velocity vorticity profiles for $\tilde{H} = 5$

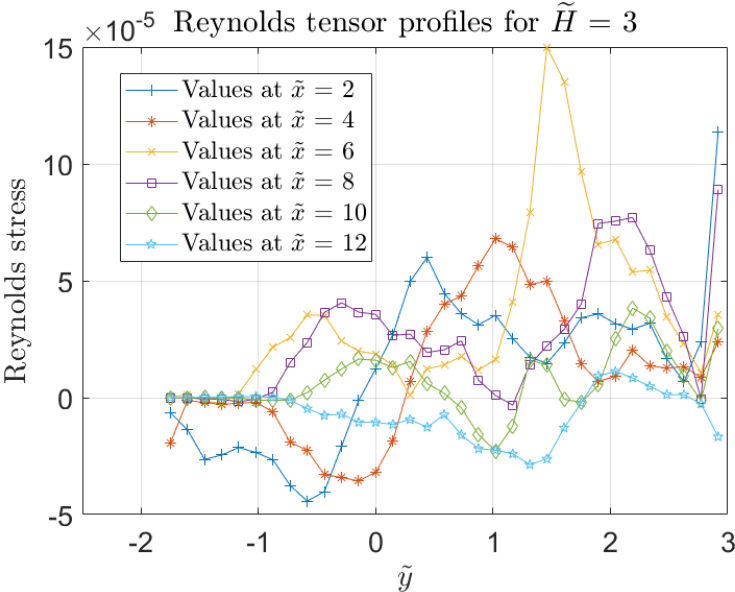


Figure 5.19: Coanda jet Reynolds tensor profiles for $\tilde{H} = 3$

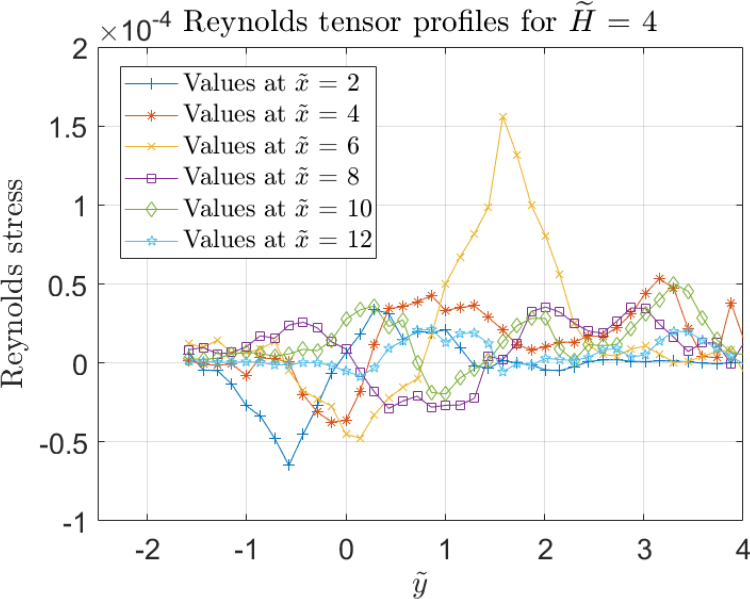


Figure 5.20: Coanda jet Reynolds tensor profiles for $\tilde{H} = 4$

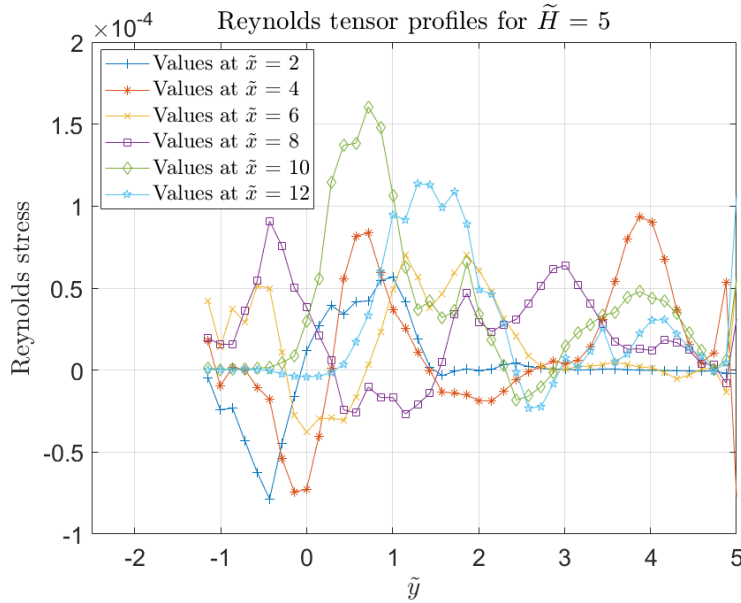


Figure 5.21: Coanda jet velocity Reynolds tensor profiles for $\tilde{H} = 5$

5.2.1 Reattachment length

Up to now, it is approximated the value of the reattachment length. But if we want to look for a more accurate definition, we can use the data of the velocity in the wall. As we observed, once the jet arrives at the wall it tends to follow it, while upstream tends to go in the opposite direction. So, if we plot u velocity component along the wall, there will be a point where the value changes its sign and this point can be defined as the reattachment point. The problem is that as we noticed previously, the values at the wall can be quite noisy, so it will be necessary to use the approximation with the streamlines to identify the range where it will be placed.

For $\tilde{H} = 3$ the u component plot comes up as it can be seen in Figure 5.22.

We know that the reattachment point is placed after $\tilde{x} = 5$ so it is clear the place where it is possible to find it in the plot. In Figure 5.23 it is applied a zoom in order to obtain a specific value. So we can conclude that the reattachment length for $\tilde{H} = 3$ is at $\tilde{x} = 6.5$.

Applying the same process for $\tilde{H} = 4$ we obtain the result seen in Figure 5.24

Here the results are more confusing and it is quite difficult to identify the

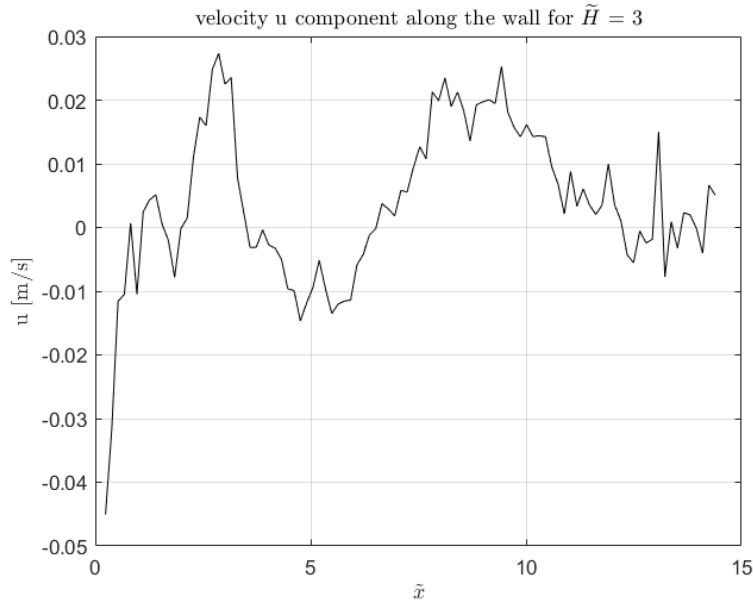


Figure 5.22: velocity u component along the wall for $\tilde{H} = 3$

correct zone. We know that the correct value is near $\tilde{x} = 9$ and, in that zone, we identify a change of tendency. Applying a zoom in that zone (see Figure 5.25) we observe that the reattachment length is at $\tilde{x} = 8.7$.

Finally for $\tilde{H} = 5$ we represent the velocity in Figure 5.26.

It is also difficult to find the value in this plot. We expect a value greater than $\tilde{x} = 10$ so, there is a zone where we have a change in the tendency. In Figure 5.27 it is applied a zoom and we conclude that the reattachment occurs at $\tilde{x} = 11.4$.

To summarize this results and compare them with the results obtained using the expression (1.1), we put all of them in Table 5.1. The same information is represented graphically in Figure 5.28.

\tilde{H}	Experimental	expression (1.1)	Statistical error
3	6.5	6.7	-2.99 %
4	8.7	8.6	1.16 %
5	11.4	10.4	9.61 %

Table 5.1: Reattachment position for the different configurations

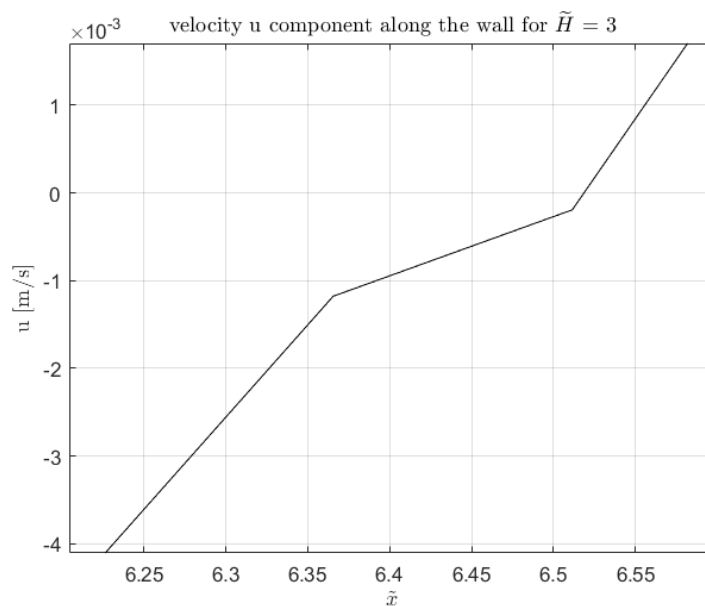


Figure 5.23: velocity u component along the wall for $\tilde{H} = 3$ (zoomed)

For the values of $\tilde{H} = 3$ and $\tilde{H} = 4$, we conclude that the values are acceptable as the error is less than the 5%. For $\tilde{H} = 5$ we observe that the error is near the 10%. This could mean that the table configuration generates a Boundary condition that affects at the desired result. For this reason, there is not continued increasing the wall distance from the output, as we would expect a greater error.

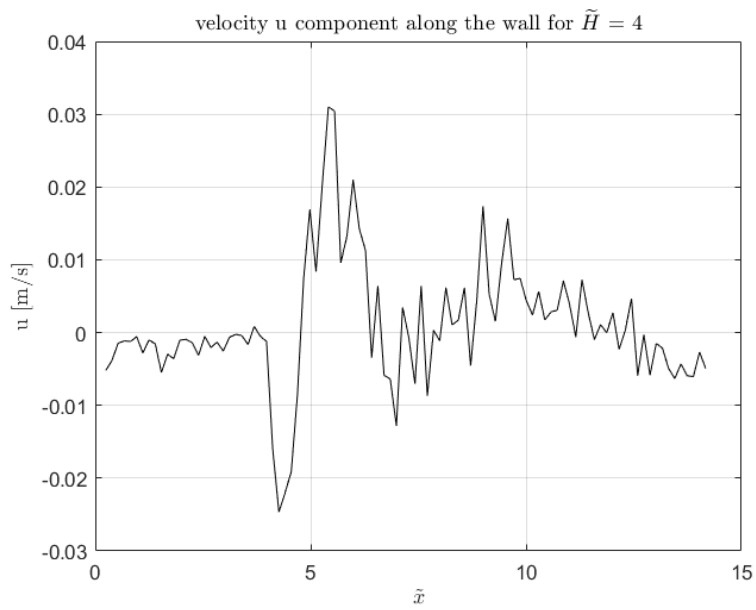


Figure 5.24: velocity u component along the wall for $\tilde{H} = 4$

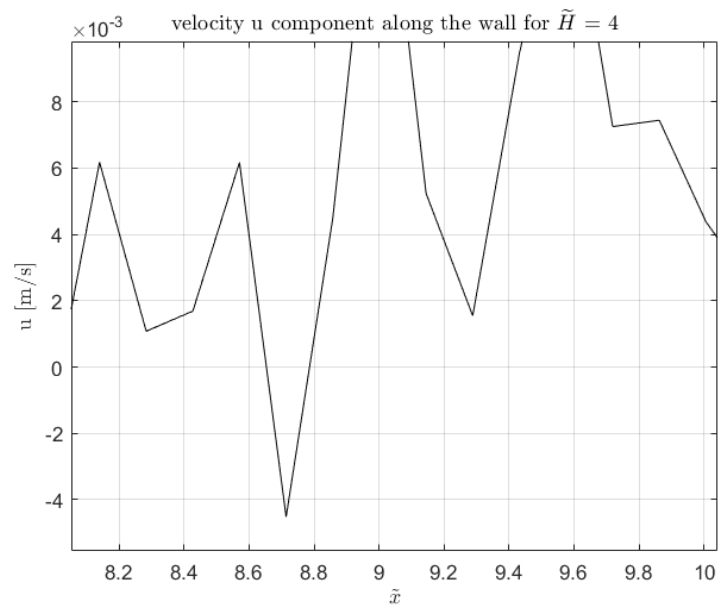


Figure 5.25: velocity u component along the wall for $\tilde{H} = 4$ (zoomed)

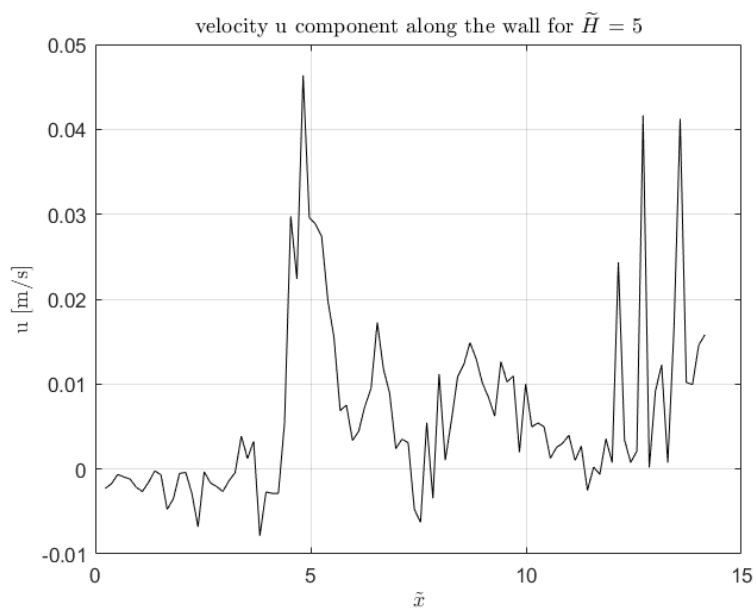


Figure 5.26: velocity u component along the wall for $\tilde{H} = 5$

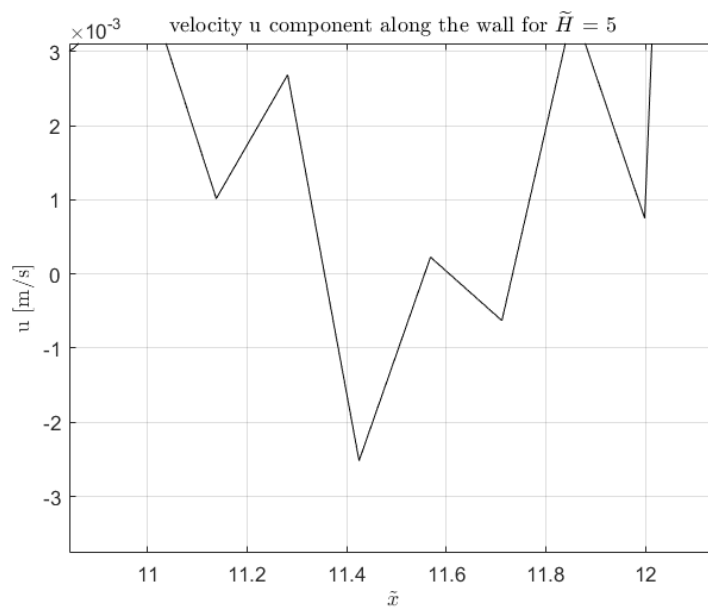


Figure 5.27: velocity u component along the wall for $\tilde{H} = 5$ (zoomed)

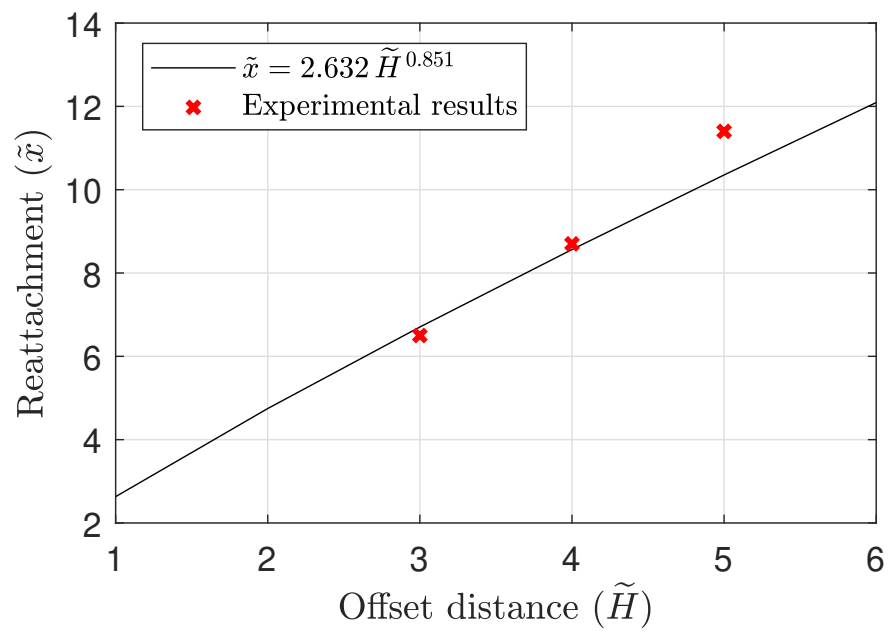


Figure 5.28: Comparison of the experimental results with expression (1.1)

Chapter 6

Conclusions

The first conclusion that we can extract after doing this thesis is the relevance of the assembly phase. It is crucial to plan correctly how to locate every component and understand their limits. For example, foreseeing that there will be a joint line in the table, it could be better to place it in a position where the camera can not capture. Then, it is important to know previously the aims of the experiment to ensure that the material is the proper one.

As we see in the results, the minimum imperfection could alter the fluid phenomenon behaviour. For that reason, one of the most important conclusions for this experiment and any other experiment of this characteristics is to really pay attention to the setup.

The next general conclusion is, that the free jet has evolved as we expected. We found some errors that in general can be fixed easily for future experiments. The most important error is the insufficient use of the spikes to turn the flow turbulent. As we want to study a turbulent jet, it is crucial to ensure that property, even if the behaviour is similar to the one expected.

About the Coanda jet, we have obtained the desired results for the first configurations but, unexpectedly, we have noticed that from the third wall distance the effect does not behave as we expected. This means that we only can reproduce the effect until the 4th wall distance. Probably the problem is that the table limit is too close to the jet outlet. Perhaps removing the boxes we can obtain better results at larger wall distances but, it will be more necessary to generate the turbulence in the channel, as the distance for the jet to evolve decrease.

Additionally, it has been proven the main objective of the thesis, to establish the influence of the wall distance in the reattachment point. We have seen

that as you move away the wall, it increases the reattachment distance. In particular, we have corroborated that the slightly non linearly relationship fits enough well in our results.

More specific conclusions of the fluid phenomenon are listed below:

- The values of the velocity are reasonable. The output mean velocity indicates that we have worked in the desired Reynolds value.
- The results present some noise that should be improved using some filters.
- Some spurious data it is presented in the wall limits that disturb the real behaviour.
- The statistical analysis coincides with the results that we can expect
- The recirculating zone is clearly identified with two counterrotating vortices.

6.1 Further work

As the final conclusion, it is suggested some further work that could be done in future experiments.

- A deep Coanda jet study, varying the Reynolds and Froude numbers to measure the sensitivity of the jet to this parameters.
- By installing a second external deposit it is possible to add another parameter as the Temperature. If we think in rivers, they have different temperatures than seas, so it is interesting to study the relevance of that fact.
- It is also possible to modify the angle respect the output of the wall. Also, by using different geometries as for example, concave and convex geometries.
- Use material with more precision in order to study smaller turbulent scales.

Bibliography

- Abramovich, G. N., Girshovich, T., Krasheninnikov, S. I., Sekundov, A., and Smirnova, I. (1984). The theory of turbulent jets. *Moscow Izdatel Nauka*.
- Adrian, R. J. and Westerweel, J. (2011). *Particle image velocimetry*. Number 30. Cambridge University Press.
- Ahmed, R., Talib, A. A., Rafie, A. M., and Djojodihardjo, H. (2017). Aerodynamics and flight mechanics of mav based on coandă effect. *Aerospace Science and Technology*, 62:136–147.
- Aloysius, S. and Wrobel, L. (2009). Comparison of flow and dispersion properties of free and wall turbulent jets for source dynamics characterisation. *Environmental Modelling & Software*, 24(8):926–937.
- Biswas, G., Breuer, M., and Durst, F. (2004). Backward-facing step flows for various expansion ratios at low and moderate reynolds numbers. *Journal of fluids engineering*, 126(3):362–374.
- Cîrciu, I. and Dinea, S. (2010). Review of applications on coandă effect. history, theories, new trends. *Review of the Air Force Academy*, (2):14.
- Eaton, J. and Johnston, J. (1981). A review of research on subsonic turbulent flow reattachment. *AIAA journal*, 19(9):1093–1100.
- Englar, R. J. (2005). Overview of circulation control pneumatic aerodynamics: Blown force and moment augmentation and modification as applied primarily to fixed wing aircraft. In *Proceedings of the 2004 NASA/ONR Circulation Control Workshop, NASA CP-2005-213509*, pages 23–66.
- Glauert, M. (1956). The wall jet. *Journal of Fluid Mechanics*, 1(6):625–643.
- Kuang, J., Hsu, C.-T., and Qiu, H. (2001). Experiments on vertical turbulent plane jets in water of finite depth. *Journal of engineering mechanics*, 127(1):18–26.

- Lalli, F., Bruschi, A., Lama, R., Liberti, L., Mandrone, S., and Pesarino, V. (2010). Coanda effect in coastal flows. *Coastal Engineering*, 57(3):278–289.
- Mi, J., Kalt, P., Nathan, G., and Wong, C. (2007). Piv measurements of a turbulent jet issuing from round sharp-edged plate. *Experiments in Fluids*, 42(4):625–637.
- Miozzi, M., Lalli, F., and Romano, G. (2010). Experimental investigation of a free-surface turbulent jet with coanda effect. *Experiments in Fluids*, 49(1):341–353.
- Nasr, A. and Lai, J. (1998). A turbulent plane offset jet with small offset ratio. *Experiments in Fluids*, 24(1):47–57.
- Nasr, A. and Lai, J. C. (2010). The effect of wall inclination on an inclined offset jet. In *Tenth International Symposium on Applications of Laser Techniques to Fluid Mechanics, Lisbon, Portugal, July*, pages 10–13.
- Pope, S. (2000). *Turbulent flows*, 771 pp.
- Raffel, M., Willert, C. E., Kompenhans, J., et al. (2007). *Particle image velocimetry: a practical guide*. Springer Science & Business Media.
- Rajasekaran, J. (2011). *On the flow characteristics behind a backward-facing step and the design of a new axisymmetric model for their study*. University of Toronto.
- Romano, G. (2016). Dispense del corso Aerodinamica sperimentale.
- Sawyer, R. (1963). Two-dimensional reattaching jet flows including the effects of curvature on entrainment. *Journal of Fluid Mechanics*, 17(4):481–498.
- Thielicke, W. (2014). PIVlab tutorial. http://pivlab.blogspot.com/p/blog-page_19.html.
- Tian, J., Roussinova, V., and Balachandar, R. (2012). Characteristics of a jet in the vicinity of a free surface. *Journal of Fluids Engineering*, 134(3):031204.
- Trancossi, M. (2011). An overview of scientific and technical literature on coanda effect applied to nozzles. Technical report, SAE Technical Paper.
- Von Glahn, U. H. (1958). Use of the coanda effect for jet deflection and vertical lift with multiple-flat-plate and curved-plate deflection surfaces.